Advances in Water Resources 97 (2016) 52–72

Contents lists available at ScienceDirect

Advances in Water Resources

journal homepage: www.elsevier.com/locate/advwatres

Filtering methods in tidal-affected groundwater head measurements: Application of harmonic analysis and continuous wavelet transform

Juan Pedro Sánchez-Úbeda[a,*], María Luisa Calvache[a], Carlos Duque[b], Manuel López-Chicano[a]

[a] Department of Geodynamics, Sciences Faculty, University of Granada, Campus Fuentenueva, E-18071, Granada, Spain
[b] Department of Geological Sciences, University of Delaware, Penny Hall, 255 Academy Street, 19716 Delaware, USA

ARTICLE INFO

Article history:
Received 9 February 2016
Revised 30 August 2016
Accepted 31 August 2016
Available online 1 September 2016

Keywords:
Tidal influence
Filtering methods
Groundwater head
Coastal aquifer
Harmonic analysis
Wavelet transform

ABSTRACT

A new methodology has been developed to obtain tidal-filtered time series of groundwater levels in coastal aquifers. Two methods used for oceanography processing and forecasting of sea level data were adapted for this purpose and compared: HA (Harmonic Analysis) and CWT (Continuous Wavelet Transform). The filtering process is generally comprised of two main steps: the detection and fitting of the major tide constituents through the decomposition of the original signal and the subsequent extraction of the complete tidal oscillations. The abilities of the optional HA and CWT methods to decompose and extract the tidal oscillations were assessed by applying them to the data from two piezometers at different depths close to the shoreline of a Mediterranean coastal aquifer (Motril-Salobreña, SE Spain). These methods were applied to three time series of different lengths (one month, one year, and 3.7 years of hourly data) to determine the range of detected frequencies. The different lengths of time series were also used to determine the fit accuracies of the tidal constituents for both the sea level and groundwater heads measurements. The detected tidal constituents were better resolved with increasing depth in the aquifer. The application of these methods yielded a detailed resolution of the tidal components, which enabled the extraction of the major tidal constituents of the sea level measurements from the groundwater heads (e.g., semi-diurnal, diurnal, fortnightly, monthly, semi-annual and annual). In the two wells studied, the CWT method was shown to be a more effective method than HA for extracting the tidal constituents of highest and lowest frequencies from groundwater head measurements.

1. Introduction

Tidal influences along shorelines produce regular fluctuations in the groundwater heads of coastal aquifers, and these influences can be used to understand the hydrogeological features of coastal areas (Erskine, 1991; Millham and Howes, 1995; Trefry and Johnston, 1998; Jha et al., 2003; Trefry and Bekele, 2004; Zhou, 2008; Chen et al., 2011; Singh and Jha, 2013). However, tidal oscillations in groundwater heads are in most cases a hindrance because they can hamper the perception of other phenomena of hydrological interest(e.g., recharge or discharge processes as river-aquifer interactions, irrigation returns and rain infiltration, or even the analysis of pumping tests). Research in coastal areas very often requires tidal filtering of the groundwater head data as a starting point, regarding the attainment of tidal constituents on the groundwater signal and the subsequent removal of tidal effects, in order to keep only the non-tidal influences on groundwater heads. Some authors have addressed this practice. Erskine (1991) presented a filtering process based on the Ferris equations (Ferris, 1952) to compensate for tidal effects by computing the tidal efficiency factor (ratio between groundwater-sea level amplitudes) and time lag (delay between a sea level oscillation and the consequent groundwater head oscillation), but the extraction of the tidal influence was incomplete. The length of the groundwater head time series was also an issue because the fit was not acceptable when tidal efficiency or time lag was applied to longer time series, and significant residual tidal fluctuations still remained in the groundwater head.

To correct pumping test data in wells close to coastlines, other authors have developed methods for removing tides. Trefry and Johnston (1998) and Chattopadhyay et al. (2015) proposed a correction to the measured pumping test drawdowns for tidal influences using least-square techniques to enable a pumping test analysis (only during the pumping period), but significant residual fluctuations still remained in the head in the first case, and in both

* Corresponding author.
E-mail addresses: juampesu@ugr.es (J.P. Sánchez-Úbeda), calvache@ugr.es (M.L. Calvache), cduque@udel.edu (C. Duque), mlopezc@ugr.es (M. López-Chicano).

http://dx.doi.org/10.1016/j.advwatres.2016.08.016
0309-1708/

cases the fits were inaccurate for longer measurement time series. Chen and Jiao (1999) fitted a regular tidal fluctuation to data from six days before a pumping test and then corrected the observed drawdowns by subtracting the tidal effect before calculating the diffusivity values. Chapuis et al. (2005) developed a theoretical equation for pumping under tidal influences and considered the tidal effects before and after the test; an admissible fit was achieved, but the test was limited to a short time series. None of those methods established a sufficiently accurate filtering methodology that accounted for the tides that produced the perturbations, durations of the datasets used, aquifer features, or study cases.

Filtering sea tidal effects is especially relevant in studies of recharge and discharge in coastal aquifers. Net inland recharges observed in mean groundwater levels in coastal areas can be overestimated due to the enhancement of mean groundwater heads by tides (Li and Jiao, 2003). In addition, tidal effects produce considerable impacts on seawater intrusion processes in mixing zones. Licata et al. (2011) simulated seawater intrusion with and without tidal effects on a mixing zone; their results indicated that tidal mixing results in more mixed pollutant and salinity concentrations than the distributions from an equivalent steady-state model without tidal effects. The methods proposed herein are expected to be useful not only in the filtering process but also for a general understanding of tidal features, their components and their effects on groundwater close to the sea in an attempt to fill in certain gaps in coastal research.

Tidal analyses are usually carried out using methods that allow periodic changes and magnitudes to be understood and predicted. Analogous methods could be used to understand the influence of tides on groundwater. Tidal motions comprise a set of components, and the two major components of sea-level time series with regard to tides (Godin, 1972) are as follows.

1. The *astronomical component*, which is due to the motion of celestial bodies and the interactions between them, is the most easily detectable and predictable.
2. The *hydrodynamic component* is due to the shape of the shoreline and the effects of perturbing factors such as winds, atmospheric pressure changes, storm events, or external inputs (e.g., river discharge into the sea).

The tidal astronomical component has the greatest frequency stability and can be decomposed into constituents (Doodson, 1954). They are tabulated in terms of their frequencies and phase angles for specific coastal locations and are commonly referred to by symbols such as *M2, S2,* and *SA* (lunar semidiurnal, solar semidiurnal, and solar annual, respectively). The hydrodynamic component of the tide is non-periodic due to its non-stationary nature, which makes its prediction more complicated (Parker, 2007). Moreover, Kacimov and Abdalla (2010) suggested that high-frequency fluctuations in sea level are already filtered by porous beach cushions, and the tidal oscillations measured in groundwater can be considered to be caused primarily by astronomical tidal forces.

Tide studies usually consist in the decomposition and adjustment of tidal components to predict their evolution (Godin, 1972; Foreman et al., 1995; Brown et al., 2012; Vianna and Menezes, 2005; Codiga, 2011; Erol, 2011). There are currently two main methodologies for processing tidal data.

(1) *Classic Harmonic Analysis (HA)* is based on a definition of sea surface elevation at one point as the sum of a finite number of sinusoids with distinct amplitudes, frequencies, and phases, where the frequencies of the earth-moon-sun system have been previously defined (Pawlowicz et al., 2002).
(2) *Continuous Wavelet Transforms (CWT)* are used to carry out a continuous analysis based on fitting a signal to a wavelet. This full group of processing tools was initially developed to represent data whose frequency contents evolve over time (Daubechies et al., 1992) and was then introduced to tidal analysis (Jay and Flinchem, 1995, 1997, 1999; Flinchem and Jay, 2000). These methods are continuously scalable in frequency and are thus versatile for use in tidal analyses, especially extraction (Erol, 2011).

The pros and cons of the two methods for decomposing tidal constituents have been widely discussed (Jay and Flinchem, 1999; Foreman et al., 1995; Matte et al., 2013). Pawlowicz et al. (2002) developed several programs in Matlab© based on classic harmonic analysis and grouped them into the ***T_TIDE*** package. There are other packages, including ***U_TIDE***, which is used to unify tidal analyses and the prediction framework (Codiga, 2011) and ***NS_TIDE,*** which was implemented by Matte et al. (2013) and adapted to the study of non-stationary signals in river tides.

In this study, the HA and CWT methods were applied to groundwater head monitoring in the proximity of the coastline affected by tides with the objective of isolating the non-tidal effects in groundwater head changes. In agreement with the conclusions of Bye and Narayan (2009), we believe that groundwater tides (i.e., the influence of tides on groundwater heads) can be represented as a sum of tidal constants in a similar manner to that in the open sea. Tides and their effects on groundwater have the same features and oscillatory shapes, and the methods therefore should be successful. To corroborate this, the tidal filtering described for tidal studies was applied in a study area in southern Spain (the Motril-Salobreña aquifer), where a set of wells with different depths near the coastline show a clear impact on groundwater monitoring.

The objectives of this study are as follows.

1. Filter the groundwater head time series from the tide-induced oscillation using HA (Codiga, 2011) and CWT (Jay and Flinchem, 1995) by adapting those oceanographic methodologies for use with groundwater and testing their applicability to hydrogeological settings.
2. Estimate the impact of the length of the monitoring time series on the results.
3. Assess other parameters that affect the data such as the depth of the monitoring wells and hydrological processes in the aquifer (e.g., recharge).

2. Hydrological settings of the study area

The Motril-Salobreña coastal aquifer extends over an area of 42 km^2 (Fig. 1A). It is comprised of detrital sediments that range from coarse gravels to sand, fine silts, and clay. The Guadalfeo River, which drains the southern Sierra Nevada, is in the western sector of the aquifer. The water budgets considered by different researchers attribute the highest inputs to river recharge (30%) and irrigation excess proceeding from river-derived water upstream (30%) (Calvache et al., 2009), the relative influences of which change depending on the season (Duque et al., 2011). In the northern sector, the aquifer is limited by the alluvium aquifer of the Guadalfeo River and a carbonate aquifer (Escalate aquifer). The southern boundary is the Mediterranean Sea. On the remaining borders, detrital rocks are in contact with schists and phyllites, which can be considered impermeable. The aquifer thickness is variable and ranges from 30 to 50 m in the northern sector (alluvial sedimentary environment) to more than 250 m in areas near the coastline (deltaic sedimentary environment) (Duque et al., 2008). The estimated hydraulic gradient ranges from 5×10^{-3} to 1.6×10^{-3} (Duque et al., 2010), and the aquifer responds very quickly to recharge due to its high permeability (Duque et al., 2011).

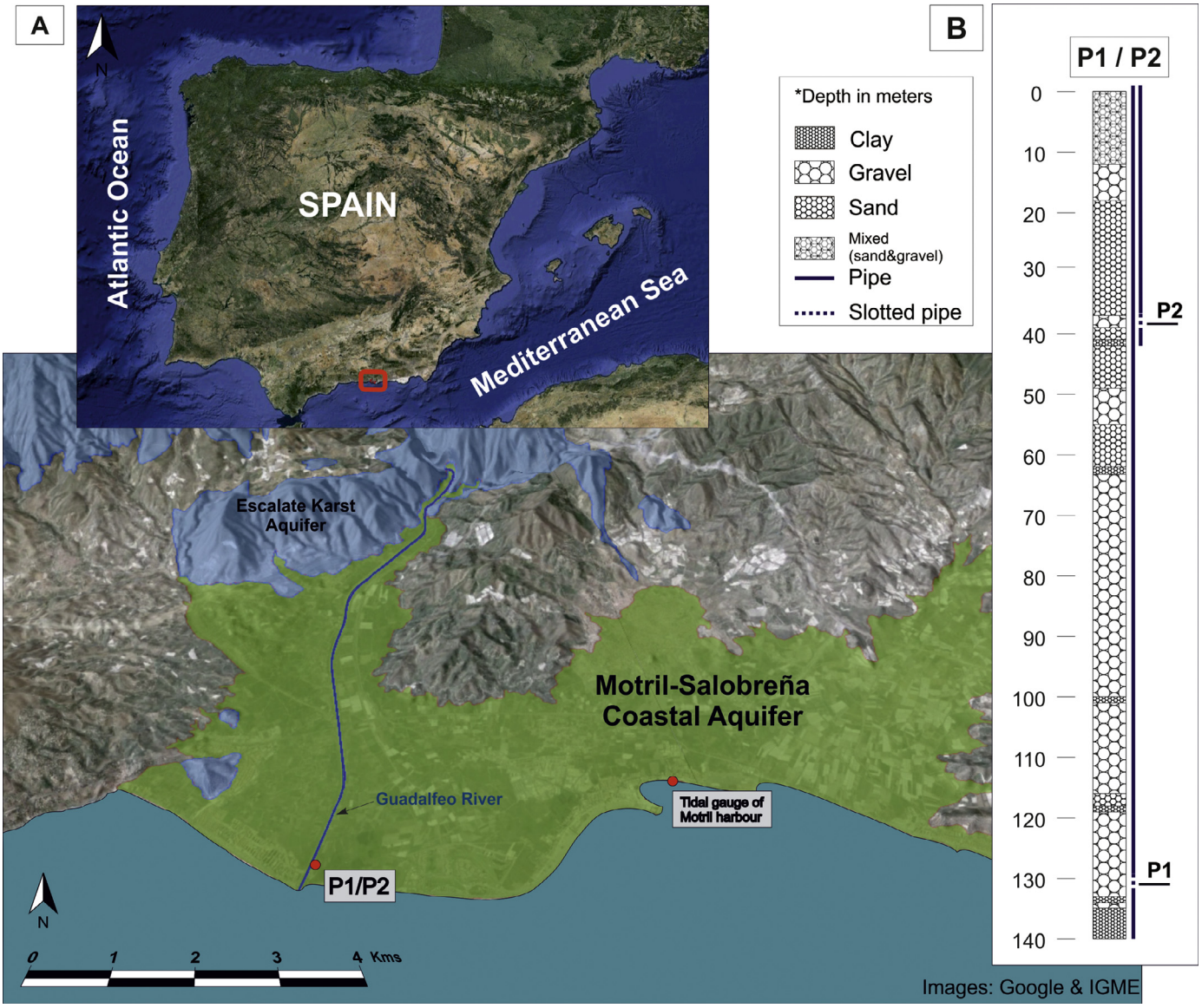

Fig. 1. (A) Location with an enlargement of the Motril-Salobreña coastal aquifer system and the mentioned study locations and the (B) hydrogeological settings at P1 and P2. (For interpretation of the references to colour in this figure legend, the reader is referred to the web version of this article.)

3. Methods

Two methods (HA and CWT) were applied to analyse the tidal influence on groundwater time series from wells in the study area. These methods were considered optimal due to the similarity of the groundwater head and sea level. For these analyses, the use of sea levels and groundwater heads was posited. The HA and CWT methods were first applied to the sea level because this process involves an initial fitting to the local tidal constituents to detect the relevance of tides on the groundwater heads and afterwards to filter them. The procedure was performed for three different time series lengths, in accordance with the second objective stated above: one month (August 2013), one year (2013), and 3.7 years (October 2010 to July 2014); the latter encompassed the entire available dataset.

The difference between the applications to the sea level and groundwater head is based on the resulting residual part of the original analysed time series, which constitutes the unperturbed groundwater head in that case. As applied to sea level, the residual part obtained is the so-called meteorological or hydrodynamic tidal component, and as applied to the groundwater head, the residual part is understood as the groundwater head that is unperturbed by tide.

Tidal information

The sea-tide level data were obtained from State Harbours (Spanish Ministry of Development) at a gauge station in nearby Motril Harbour (Fig. 1A), where tide data were monitored every five minutes. The data were cleaned by applying a 54-point symmetric filter to eliminate energy at high frequencies, noise in the measured signal, and instrumental errors (above 0.5 cph); the data were resampled at hourly time intervals, which left only those oscillations with periods greater than 1 h. The general expression of this type of filter is

$$X_f(t) = \mathcal{F}_0 X(t) + \sum_{m=1}^{M} \mathcal{F}_s [X(t+m) - X(t-m)], \quad (1)$$

where $X_f(t)$ is the filter value at time t, $\mathcal{F}_0$ are the filter coefficients, $X(t)$ is a single data point at time t, and $\mathcal{F}_s$ is the cut-off frequency (low-pass filter), with $M = 54$ points in this case.

Groundwater head information

An hourly sampling rate database was used for two points 300 m landwards from the shoreline (Fig. 1A), which corresponded to wells P1 and P2; the piezometers were at different depths (132 m and 38 m below mean sea level, respectively). Both datasets were assumed to have been logged at the same point but at different depths because the distance between them was only 3 m (Fig. 1B). The groundwater heads were first corrected in time to GMT+00 and normalized to their averages (for each time interval, the mean was removed) to allow an easier comparison of the graphs. The time series were then noise-filtered to eliminate peaks or measurement errors at high frequencies, as in the sea level data, thus improving the tidal detection.

3.1. Harmonic analysis applying U_TIDE

The ***U_TIDE*** code was used for the HA analysis. It determines the phase and amplitude coefficients of *a priori* known tidal frequencies via a least squares fitting procedure. The simplest form of the model equation used for the one-dimensional case (applied in the present study) in ***U_TIDE*** is (Codiga, 2011)

$$X^{mod}(t_i) = \sum_{q=1}^{n_{allc}} \left(E_{iq} \cdot a_q\right) + \bar{X} + \dot{X}\left(t_i - t_{ref}\right), \tag{2}$$

where X^{mod} is the modelled signal (tide level or groundwater head in this case) at each time (t_i), for $i = 1 \ldots n_t$ (n_t is the last time step). The sum represents all the tidal constituents detected from $q = 1 \ldots n_{allc}$ (n_{allc} is the sum of all the constituents). Each constituent has constant amplitude a_q, which is multiplied by the exponential function E_{iq}. The mean $\bar{X}$ and the trend $\dot{X}$ (if included) are also computed in the model relative to the reference time, $t_{ref} = (t_1 + t_{n_t})/2$, which is the average time expressed as the central time from the raw input time, from t_1 to t_{n_t}. The exponential function E_{iq} represents the pre-filtering and nodal/satellite corrections, which are counter clockwise and clockwise-rotating elements that the complex coefficients multiply (applied for each q constituent at each i time) in the form

$$E_{iq} = E(t_i, \omega_q) = P(\omega_q) \cdot F(t_i, \omega_q) \cdot \exp i(U(t_i, \omega_q) + V(t_i, \omega_q)) \tag{3}$$

where $P(\omega_q)$ is a correction factor for optional pre-filtering (set to unity in the case of no pre-filtering), $F(t_i, \omega_q)$ (unitless) is the nodal/satellite correction amplitude factor (set to unity in the case of no pre-filtering), $U(t_i, \omega_q)$ (radians) is the phase offset (set to zero in the case of no pre-filtering), and ω_q is the radian frequency of each individual harmonic constituent. $V(t_i, \omega_q)$ (radians) is the astronomical argument, which ensures that the resulting phase lags are relative to the equilibrium tide at Greenwich (applied in this study). The amplitude expression is

$$a_q = A_q \exp i(g_q). \tag{4}$$

A_q are the real magnitudes of the amplitudes, and the g_q are the associated Greenwich phases for all the amplitudes of each constituent.

The relation of the above expressions to the real formulation is valuable for understanding the one-dimensional analysis. The model Eq. (2) is the expression for the real-valued components of the qth constituent (non-reference, reference, or inferred):

$$\eta_q^{mod}(t_i) = A_q^{\eta} P_q F_{iq} \cos\left(U_{iq} + V_{iq} - g_q^{\eta}\right) + \bar{\eta} + \dot{\eta} \cdot \left(t_i - t_{ref}\right), \tag{5}$$

where q represents any of the constituents, and i is the time. A_q^{η} and g_q^{η} are the real-valued amplitude and Greenwich phase lag of the respective component. The real-valued cosine and sine coefficients are defined as

$$X_q^{\eta} = A_q^{\eta} \cos g_q^{\eta} \text{ and} \tag{6}$$

$$Y_q^{\eta} = A_q^{\eta} \sin g_q^{\eta}, \tag{7}$$

and the relations to the amplitude and Greenwich phase lag are

$$A_q^{\eta} = \sqrt{X_q^{\eta^2} + Y_q^{\eta^2}}, \text{ and} \tag{8}$$

$$g_q^{\eta} = arctan\left(Y_q^{\eta}, X_q^{\eta}\right). \tag{9}$$

The real and imaginary parts of the functions therefore are

$$X_q = X_q^{\eta} = 2Re(a_q), \text{ and} \tag{10}$$

$$Y_q = Y_q^{\eta} = 2i\ Im(a_q). \tag{11}$$

A fitting using the *IRLS* algorithm (iteratively reweighted least squares) was added to the successive changes as an extension of the ordinary least squares calculation of the harmonic analysis, which is more resistant to broad spectrum noise, hence increasing the confidence in the computed parameters and also allowing more low-amplitude constituents to be resolved from the background noise (Leffler and Jay, 2009). In a general sense, the tidal forcing is modelled as a sum of a finite set of sinusoids at different (previously fixed) frequencies. These frequencies are specified by various combinations of sums and differences of integer multiples of six fundamental frequencies arising from planetary motions (Godin, 1972). The six signed integers that are required to describe a particular frequency are called the Doodson numbers (Doodson, 1954) and constitute the astronomical part of the tide. The phase values obtained for each component are relative to Greenwich, that is, the phase referenced to the phase of the equilibrium response at 0° longitude (Greenwich meridian). The nodal corrections are computed and applied to an amplitude and phase relative to the exact time (Greenwich Time for a latitude of 36.733°).

To run the ***U_TIDE*** code, the levels are introduced as input vectors of hourly sampled data, identical to that of the sea level. However, in this case, the fit obtained by the code entering the groundwater head must be recognized as the tidal part that affects the groundwater head, which corresponds to the astronomical component of the tide, and the residual part is the filtered groundwater head (the non-tidal part of the groundwater head).

3.2. Continuous wavelet transform method

Regarding the interpretation of the tidal frequencies, because there are no pre-fixed frequencies, the CWT has several differences with respect to HA, and representing the original data as completely and compactly as possible is emphasized (Flinchem and Jay, 2000). This means that the CWT method focuses on the reconstruction of the raw input, in contrast to the HA method, which finds within the raw input all the recognizable tidal constituents based on the pre-fixed frequencies for each one. In the present study, the CWT method was applied using predefined functions in Matlab© such as the Continuous Wavelet Transform using fast Fourier Transform Algorithm (*cwtft*) for detecting and fitting processes and the Inverse Continuous Wavelet Transform (*icwtft*) for the specific reconstruction of the original signal, among others. The code used was partially implemented in Matlab© by the authors and included some portions and concepts from other studies that are cited here; however, the mathematical basis is explained below. A definitive code that implements the complete filtering process is still under development.

The definition of a CWT (Flinchem and Jay, 2000) begins with the choice of an oscillatory prototype function (wavelet) $\Psi_0(t)$, which has a finite variance, is localized in time near the origin and

has zero mean:

$$\text{a)} \int \Psi_0(t)\Psi_0*(t)\,dt<\infty,\ \text{b)}\ \lim_{t\to\infty}\Psi_0(t)=0,\ \text{and c)}\ \int \Psi_0(t)dt=0. \tag{12}$$

The analysing function is a wavelet Ψ, and the CWT process compares the signal to shifted and compressed (or stretched) versions of that wavelet (Jay and Flinchem, 1999).

For a scale parameter $a > 0$ and position b, the CWT can be expressed as the inner product of a signal $f(t)$ with translated and dilated versions of an analysing wavelet $\Psi(t)$:

$$C\,(a, b; f(t), \Psi(t)) = \int_{-\infty}^{\infty} f(t)\frac{1}{\sqrt{a}}\Psi^*\left(\frac{t-b}{a}\right)dt, \tag{13}$$

where $*$ denotes the complex conjugate, the scale a is the inverse of frequency ω ($0 < a = \frac{1}{\omega} < \infty$), and b is the translation from the origin ($-\infty < b < \infty$) along the localized time index t. The CWT can also be interpreted as a frequency-based filtering of the signal by rewriting it as an inverse Fourier transform:

$$C(a, b; f(t), \Psi(t)) = \frac{1}{2\pi}\int_{-\infty}^{\infty}\hat{f}(\omega)\sqrt{a}\left(\hat{\Psi}(a\omega)\right)^* e^{j\omega b}d\omega, \tag{14}$$

where $\hat{f}(\omega)$ and $\hat{\Psi}(\omega)$ are the Fourier transforms of the signal and wavelet, respectively. The CWT acts as a bandpass filter on the input signal at different scales. By continuously varying the values of the scale parameter a and the translation parameter b, the CWT coefficients $C\,(a, b)$ are obtained. The application of Eqs. (13) and (14) requires that a and b are discretized, with a chosen to match the tidal frequencies. To express the CWT as a convolution from Eq. (14), we define

$$\hat{\Psi}_a(t) = \frac{1}{\sqrt{a}}\Psi^*(-t/a) \tag{15}$$

and rewrite the wavelet transform as

$$\left(f * \hat{\Psi}_a\right)(b) = \int_{-\infty}^{\infty} f(t)\hat{\Psi}_a(b-t)dt. \tag{16}$$

Thus, the CWT of a discrete sequence x_n is defined as the convolution of x_n with a scaled and translated version of $\Psi(t)$ (Torrence and Compo, 1998):

$$W_a[b] = \sum_{n=0}^{N-1} x[n]\hat{\Psi}_a[b-n]. \tag{17}$$

Computing the convolution for each value of the shift parameter b and repeating the process for each scale a, we can obtain the CWT.

Consistent with (12), a non-analytic Morlet wavelet is employed here, which is defined in the Fourier domain by

$$\hat{\Psi}(a\omega) = \pi^{-1/4}\{e^{(a\omega-\omega_0)^2/2} - e^{\omega_0{}^2/2}\}, \tag{18}$$

where ω_0 is the nondimensional frequency, which had a default value of 6 to satisfy the admissibility condition from Eq. (12a) (see (Farge, 1992) for more details on Morlet wavelets).

The number of scales ($NbSc$) is determined by the following equation (default values in Matlab© for Morlet wavelets):

$$NbSc = (log_2(N)/ds) + 1, \tag{19}$$

where N is the length of the input signal. The smallest resolvable scale is $2{*}dt$, where dt is the sampling period, and the default spacing between scales (ds) for the Morlet wavelets is equal to 0.4875. In this case, a non-linear scale vector is needed, so the type of spacing between scales is defined as

$$S_0 * pow. \wedge ((0\,\text{to}\,NbSc-1) * ds), \tag{20}$$

where S_0 is the smallest scale. This results in a constant spacing of ds if the logarithm is taken to the base power of the scales vector.

3.3. Selection of tidal constituents in U_TIDE based on the HA method

For the HA analysis, the constituents included in the model were evaluated (in terms of its significance within the entirety of constituents) using an automatic decision tree (Foreman, 1977) to choose the major tidal constituents based on the signal-to-noise ratio (SNR) and Percent Energy (PE). The SNR factor is the squared ratio of the amplitude to the error in the amplitude:

$$SNR_q = (A_q/\epsilon_q)^2. \tag{21}$$

The relative importance of a constituent in terms of its significance is also gauged by the Percent Energy (PE), in an amplitude-weighted sense (Codiga and Rear, 2004):

$$PE_q = 100\frac{E_q}{\sum_{q=1}^{n_{allc}} E_q}, \tag{22}$$

where E_q is the energy associated with constituent q, and the sum of the E_q values is equal to 100. The values of the Percent Energy factor (PE) are obtained as an output of ***U_TIDE***, which is useful for ranking the constituents so that the importance of the constituents in an amplitude-weighted sense is clear (Codiga, 2011). In summary, when the results for each time series length under study are obtained, the main tidal constituents are chosen or omitted according to their diagnostics, which assess the constituent significance of each constituent as determined by the SNR and PE factors. The tidal constituents that were detected by the code to have amplitudes greater than 0.001 m were taken into account, but the code used the terms described above to evaluate the chosen constituents.

The diagnostics related to the constituent independence were evaluated using the Rayleigh criterion, which is traditionally used with HA (Foreman, 1977), and the modified Rayleigh criterion (Codiga, 2011). The conventional expression of the Rayleigh criterion in that case is

$$R^R(q_1, q_2) = \left(\frac{LOR_e}{1/|\omega_{q_2} - \omega_{q_1}|}\right)/R_{min} \geq 1. \tag{23}$$

where R_{min} is the minimum threshold that was taken to be 1 in that case, which is equivalent to requiring that the *effective length of the record* is sufficiently long to resolve the two frequencies from each other (Codiga, 2011) and is defined as

$$LOR_e = (n_t/(n_t-1))LOR, \tag{24}$$

where LOR is the length of the record, and the frequency resolution is $\Delta\omega = 1/LOR_e$. In the case of evenly spaced times with time separation Δt, $LOR_e = n_t \cdot \Delta t$.

Accordingly, the noise-modified Rayleigh criterion for constituent q_1 relative to constituent q_2 is defined as

$$R^{NM}(q_1, q_2) = \left(R^R(q_1, q_2)\sqrt{(SNR_{q_1} + SNR_{q_2})/2}\right) \geq 1. \tag{25}$$

Finally, the diagnostic that characterizes the fits reconstructed by U_TIDE is based on the percentage of tidal variance (Codiga, 2011), following model Eq. (2):

$$\begin{aligned} PTV_{allc} &= 100\,\frac{TV_{allc}}{TV_{raw}} = 100\,\frac{\left|X^{\,mod} - \overline{X}\cdot I(n_1, l) - \dot{X}\cdot t\right|^2}{\left|X^{raw} - \overline{X}\cdot I(n_1, l) - \dot{X}\cdot t\right|^2} \\ &= 100\,\frac{\left|\sum_{q=1}^{n} E_{iq}a_q\right|^2}{TV_{raw}}, \end{aligned} \tag{26}$$

where TV_{allc} and TV_{raw} (each in units of squared raw input units) are the tidal variances after removal of the mean and trend (if removed) of the (all-constituent) model solution and the raw input,

respectively. For reconstructions that meet the SNR significance criterion (*snrc*), the percentage of tidal variance of the corresponding reconstructed fit is

$$PTV_{snrc} = 100\,\frac{TV_{snrc}}{TV_{raw}}. \tag{27}$$

The percentages of tidal variance provide an idea of how much signal could be caused by tide. All the detected constituents are used to determine Eq. (26), but only the constituents that satisfy the *snr* factor are used in Eq. (27).

3.4. Selection of tidal constituents in the CWT method

In the CWT method, the frequencies that may be resolved in a record are determined using the Heisenberg uncertainty principle:

$$\sigma_\omega \sigma_\tau \geq (4\pi)^{-1}, \tag{28}$$

where σ_ω is the uncertainty in frequency, and σ_τ is the uncertainty in time. This defines what may be simultaneously and consistently asserted about the frequency and time localization or extent of a process represented as a wave. It is therefore the most fundamental restriction on the frequency resolution of any form of tidal analysis, so that frequency resolution is better at low frequencies, where the window is longer (Landau and Lifschitz, 1977; Jay and Flinchem, 1999). Further, the time and frequency resolutions are functions of scale, and the information for each specific frequency does not depend on the nearest frequencies (Jay and Flinchem, 1999).

This affirmation can be observed in the general change in the frequency-band sharpness between different time periods in the spectra of each time series length used (month, year, and 3.7 years) (Fig. 2). When the analysed time series is longer, the tidal bands are shown as well-defined windows wherein the set of constituents around a specific period is clearly detectable. Conversely, with shorter analysis windows, these bands are more scattered, but the energy associated with each one (*y*-axis) is higher for shorter periods.

The CWT procedure allows the relative frequency uncertainty to be conserved, which makes the time-frequency relation of the Heisenberg principle constant. These characteristics determine the selection of frequency bands that are localized at major tidal frequencies by this method. The selection consists in the fitting of the frequency bands that have been matched with the tidal frequencies for each time series length of tide data.

The general correspondence between scale and frequency (see the Matlab© help for *Scale and Frequency*) is: Low scale => Compressed wavelet => Rapidly changing details => High frequency, and, on the other hand, High scale => Stretched wavelet => Slowly changing, coarse features => Low frequency. Nevertheless, no precise relationship exists between scale and frequency, and it is therefore usual to talk about pseudo-frequency corresponding to a scale. The scale-frequency Fourier factor relation for a Morlet wavelet is

$$\frac{4\pi a}{\omega_0 + \sqrt{2+\omega_0^2}}, \tag{29}$$

where a is the scale, and ω is the frequency. This expression was applied to visualize the scale-frequency relation in terms of the frequency bands associated with tidal frequencies in a range, which are denominated tidal species.

Stretching or compressing a function is collectively referred to as dilation or scaling and corresponds to the physical notion of scale. As Parker (2007) stated, the CWT method does not use tidal constituents but instead uses only tidal species, usually the semidiurnal band, the diurnal band, the higher harmonic (over tide) bands and, occasionally, the subtidal bands (fortnightly and monthly). These major bands are detected at different scales (pseudo-frequencies) and with a specific position.

It is known from CWT that the results in one frequency band are independent of those in other bands, so that the frequency responses of a CWT analysis using a series of wavelet filters are well-defined functions (Jay and Flinchem, 1999). In summary, this approach is applied to bandpass filter the input data, where lower scales represent energy in the input data at higher frequencies, and higher scales represent energy in the input data at lower frequencies. However, unlike Fourier bandpass filtering, the width of the bandpass filter in the CWT is inversely proportional to scale.

The process for selecting the tidal frequencies is simply to match the frequencies of the principal tidal constituents (the known astronomical forcing of the local tide) with the detected bands (scales) of those tidal frequencies in the groundwater head. Thus, the main tidal bands were fitted based on the frequency distribution of tidal bands (Guo et al., 2015), with specific ranges of 0.0357–0.0463 (cycles per hour or cph) for the diurnal band (D1), 0.0734–0.0879 (cph) for the semidiurnal band (D2), and 0.1553–0.1697 (cph) for the quarterdiurnal band (D4).

This process is applied, as in the application of the HA method, to both the tide level and measured groundwater head. However, the outputs in this case differ from the HA method, and the detection process for the frequency bands simply involves a comparison between the tidal frequency bands (at our specific location) and frequency bands detected in the groundwater head to ascertain that the fit of the tidal bands is complete and locally consistent for their subsequent extraction.

4. Results

The groundwater heads in wells P1 and P2 were clearly affected by the tide (Fig. 3). The mean amplitude of the tide in the Mediterranean Sea at the Motril coastline is 0.54 m, and its influence on the groundwater head led to amplitudes of 0.3 m and 0.18 m at P1 and P2, respectively. The 300 m distance from the shoreline to P1 and P2 produced those attenuations, which were defined as decays in the tidal amplitudes (Erskine, 1991; Cartwright et al., 2003; Bye and Narayan, 2009). The time lags between the tide and its effect on the groundwater heads in P1 (1.056 h) and P2 (1.224 h) reflected the travel time through the coastal fringe of the aquifer (Erskine, 1991). The values were calculated directly from the comparison of the datasets as delays between two different periodic signals, regardless of each tidal constituent. However, the easiest way to calculate the delay between two signals is to compare the most remarkable oscillations in the signals, which in this case are the semidiurnal constituents.

The P1 and P2 time series show the main tidal oscillations (attenuated) and the non-tidal oscillations, the latter of which may be related to the principal inland groundwater changes (rainfall recharge, differential river recharge, irrigation return or nearby pumping activity). Those processes can cause non-periodic groundwater level changes, which turn the signal into a complex sum of different non-stationary components and hinder its evaluation. However, the tidal perturbations in the groundwater head measurements could still be determined, even when the tidal influence was rather small and the non-tidal changes presented a high magnitude.

The groundwater time series showed tidal constituents that included the semidiurnal and diurnal frequencies and the moon fortnightly and moon-solar fortnightly constituents (spring and neap tides) in one month; both are visible in Fig. 3. The main constituents are the semidiurnal and diurnal ones, and the fortnightly tide is less than 0.56% of the total mean amplitude (0.003 m of 0.54 m). Those frequencies were previously known to be part of the astronomical tide. The fitted tidal portion within the ground-

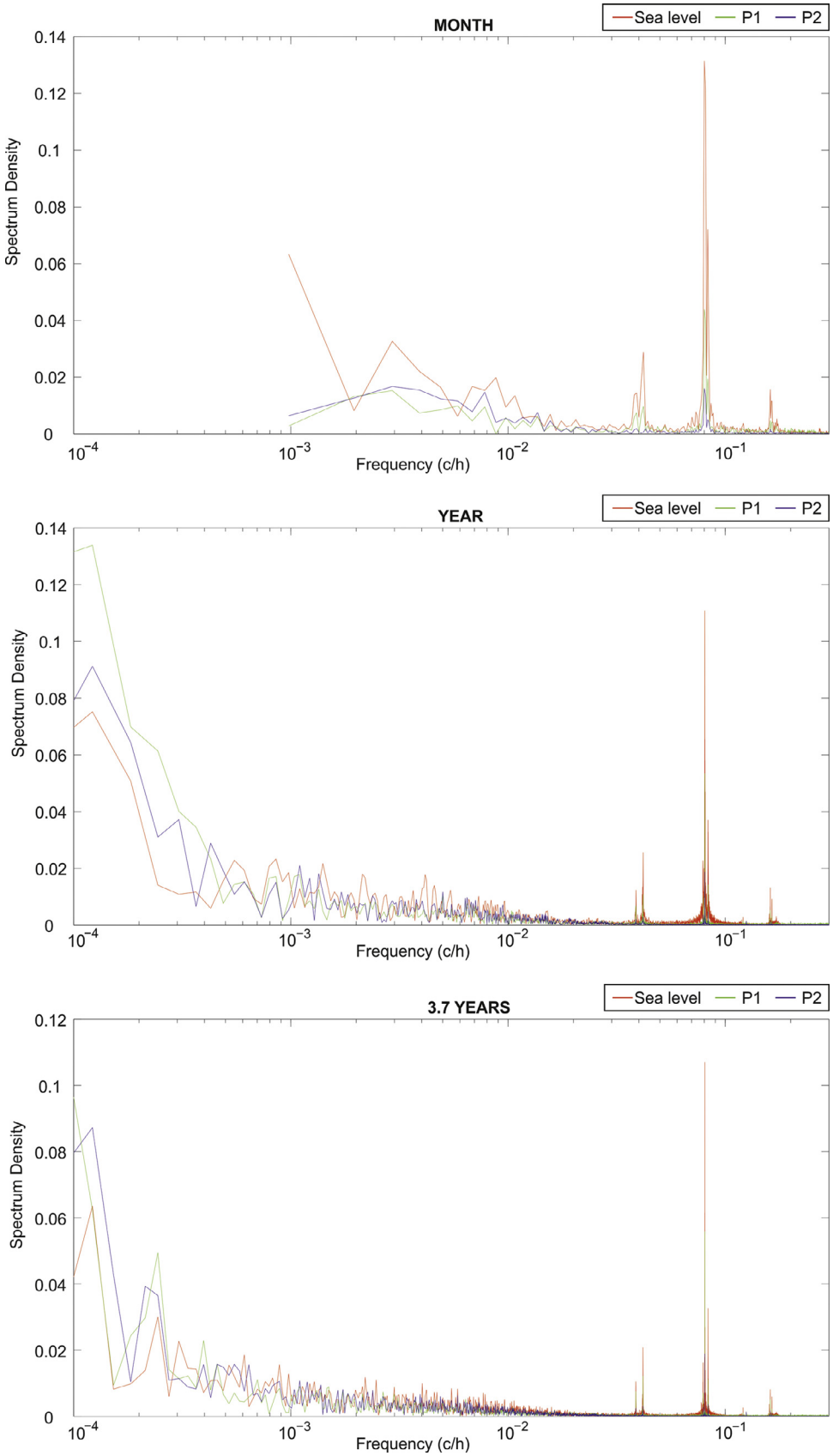

Fig. 2. Density spectra (energy versus frequency) for one month (A), a year (B), and 3.7 years (C) of the sea level and groundwater heads at P1 and P2. (For interpretation of the references to colour in this figure legend, the reader is referred to the web version of this article.)

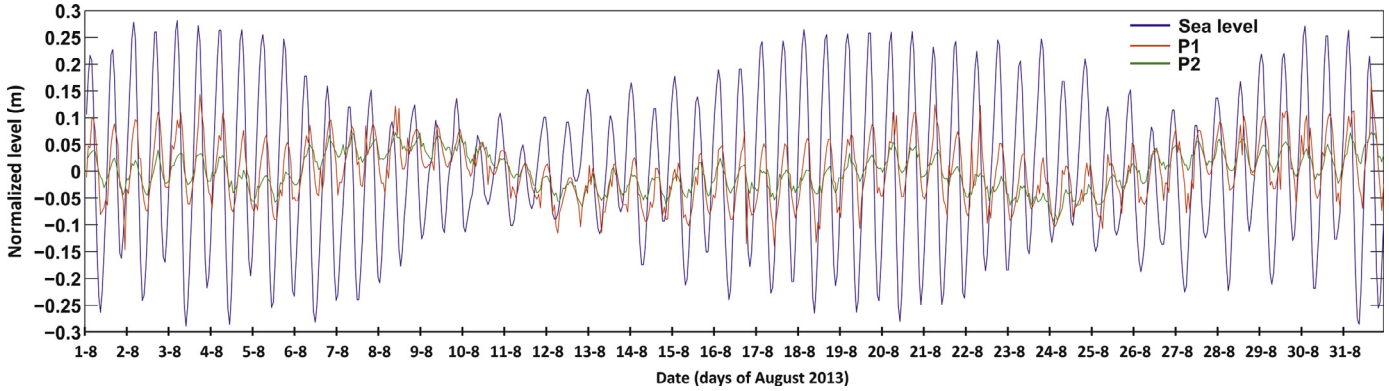

Fig. 3. Sea level (blue line), groundwater head at P1 (red line), and at P2 (green line) for one month (August 2013). The principal astronomical tidal oscillations (diurnal, semidiurnal, and fortnightly periods) and the differences in amplitude due to the depth of monitoring can be readily recognized. (For interpretation of the references to colour in this figure legend, the reader is referred to the web version of this article.)

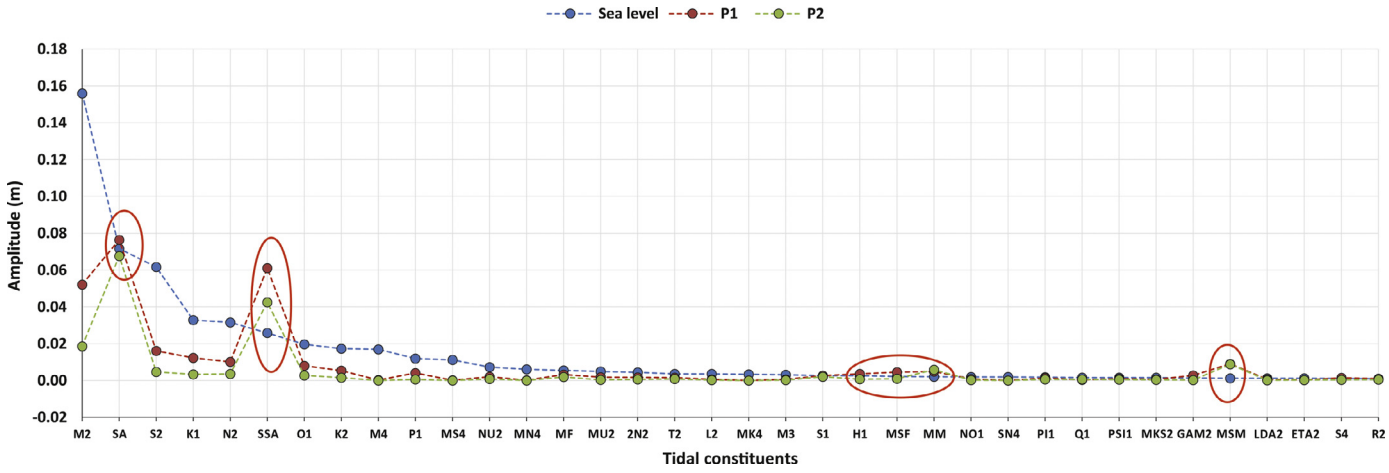

Fig. 4. Fitted amplitude of each tidal constituent in 3.7 years at P1 (A) and P2 (B), together with fitted tidal constituents (in the order of the PE values for the sea level). The lower frequencies in each case show higher errors in fitting, such as the SA, SSA, MSM and MM constituents (red circles). (For interpretation of the references to colour in this figure legend, the reader is referred to the web version of this article.)

water head can be attributed to non-tidal forces. It is assumed that the hydrodynamic tidal component (the non-astronomical forces of the tide) is negligible, and so is its effect on the groundwater head at 300 m from the coastline, where these high-frequency sea level fluctuations are already filtered, as noted by Kacimov and Abdalla, (2010). Therefore, all the tidal constituents fitted in the groundwater time series were considered to be caused by the astronomical tide, and the residual part must be the filtered groundwater head. This assumption also includes the perturbations associated with the non-linear variations, which may be considerable in groundwater head measurements close to coasts (Teo et al., 2003), but the tide is presumed to be strongly filtered and modulated 300 m from the shoreline (by the aquifer in this case). Furthermore, over-height effects associated with tidal forces may occur in this coastal situation (Nielsen, 1990; Wu, 2009). Additional comments regarding these questions can be found in the Discussion.

4.1. Fitting and filtering of the tidal portion using the HA-based method

The main astronomical tidal constituents (semidiurnal, diurnal, and fortnightly periods) can be readily recognized. For each constituent, both the PE and SNR parameters were adjusted and used in the automatic selection of the constituents. The amplitudes (A), phase angles (g), and the 95% confidence intervals of both (A_ci and Ph_ci) also were calculated and are shown in Table 1A (for tide), B (for P1), and C (for P2).

The tidal constituents of the sea gauge fitted for the complete available time series, one year and one month are shown in Table 1A. Those constituents accounted for approximately 97% of the total energy of the tide records in all cases (time series lengths), and the same constituents were evaluated in both the P1 and P2 head records (Table 1B and C, respectively), but the total justified energy was lower because, in addition to the tidal influence, there was more non-tidal energy.

The HA method provided fits of the tidal variance with all the detected constituents (*PTVallc* in Table 1A, B, and C) for the tide records of 77.7%, 76.5%, and 96.8% (for the 3.7 year, one year, and one month durations, respectively). The values in P1 decreased to 13.6%, 23%, and 86.5%, and in P2 they varied from 14.9%, 20%, and 47.7%, respectively. This variability suggests that the analysis of the number of detected constituents was heavily influenced by the lengths of the time series (both for the tide and piezometers, depending on the time series considered).

The number of frequencies that can be fitted are directly determined by the length of the time series, since a length at least two times the period of the lowest detectable frequency is necessary. Furthermore, the proper detection of a specific tidal constituent (close to a specific frequency) depends on the number of times that it appears in the analysed signal, and the higher fre-

Table 1
(A-B-C). Diagnostic results obtained by the HA method (***U_TIDE***) for 3.7 years, one year, and one month at sea level (A), the P1 head (B), and the P2 head (C). All the values are the detected principal tidal components (with **A ≥ 0.001**). **NAME**: Darwin Nomenclature; **PE**: Percent Energy (%); **SNR**: Signal to Noise Ratio; **A**: Amplitude (m); **A_ci**: 95% confident interval for the amplitude; **Ph**: Greenwich phase lag (°); **Ph_ci**: 95% confidence interval for the Greenwich phase lag.

Sea tide results for 3.7 years							Sea tide results for 1 year							Sea tide results for 1 month						
NAME	PE	SNR	A	A_ci	Ph	Ph_ci	NAME	PE	SNR	A	A_ci	Ph	Ph_ci	NAME	PE	SNR	A	A_ci	Ph	Ph_ci
M2	0.6494	890,000	0.1560	0.0003	48.1	0.129	M2	0.7038	260,000	0.1550	0.0006	47.8	0.259	M2	0.7763	14,000	0.1660	0.0028	175	1.05
SA	0.1362	1300	0.0716	0.0039	249	2.54	S2	0.1132	31,000	0.0620	0.0007	73.5	0.584	S2	0.1452	2000	0.0718	0.0031	110	2.34
S2	0.1012	130,000	0.0617	0.0003	73.7	0.365	SSA	0.0683	91	0.0482	0.0099	15.8	9.78	K1	0.0262	1900	0.0305	0.0014	185	2.71
K1	0.0288	68,000	0.0329	0.0002	153	0.468	K1	0.031	27,000	0.0324	0.0004	155	0.689	N2	0.0227	480	0.0284	0.0026	71	5.57
N2	0.0266	28,000	0.0316	0.0004	31.4	0.576	N2	0.0305	11,000	0.0322	0.0006	30.4	1.35	O1	0.0116	770	0.0203	0.0014	240	3.71
SSA	0.0177	150	0.0258	0.0041	62.7	7.76	O1	0.0106	8400	0.0190	0.0004	121	1.1	M4	0.0075	260	0.0163	0.0020	62.3	6.79
O1	0.0103	22,000	0.0197	0.0003	121	0.891	K2	0.0097	3000	0.0181	0.0007	65.7	2.2	MS4	0.006	240	0.0146	0.0019	35.8	6.84
K2	0.008	9900	0.0173	0.0003	68.9	1.04	M4	0.0082	5500	0.0167	0.0004	162	1.4	MSF	0.0023	5.8	0.0091	0.0074	247	53.6
M4	0.0076	29,000	0.0169	0.0002	161	0.737	MM	0.0051	9	0.0131	0.0086	161	44.3	MN4	0.0009	34	0.0056	0.0019	290	18.3
P1	0.0038	8600	0.0119	0.0003	150	1.13	P1	0.0049	3600	0.0129	0.0004	147	1.78	ETA2	0.0004	7.5	0.0037	0.0026	5.65	93.8
MS4	0.0033	18,000	0.0112	0.0002	225	1.05	MS4	0.0041	3300	0.0118	0.0004	226	2.09	M3	0.0002	22	0.0028	0.0012	208	25.4
NU2	0.0014	1600	0.0072	0.0004	32.4	2.63	MF	0.0038	6	0.0114	0.0091	188	47.8	OO1	0.0002	8.6	0.0025	0.0016	335	33.4
MN4	0.001	4600	0.0061	0.0002	119	1.76	NU2	0.0013	300	0.0066	0.0007	45.1	5.73	MO3	0.0002	18	0.0024	0.0011	230	26.6
MF	0.0008	6.8	0.0055	0.0041	144	43.9	MN4	0.0009	650	0.0056	0.0004	121	3.73	S4	0.0001	3.1	0.0016	0.0018	18	95.9
MU2	0.0006	720	0.0049	0.0004	3.99	4.23	2N2	0.0005	170	0.0041	0.0006	30.1	8.72	UPS1	0.0001	5.1	0.0015	0.0013	332	60.4
2N2	0.0005	700	0.0044	0.0003	11.3	4.45	MU2	0.0005	140	0.0040	0.0006	12.4	8.6	NO1	0.0001	4	0.0014	0.0013	39.4	68.2
T2	0.0004	440	0.0037	0.0003	79.8	5.86	L2	0.0004	120	0.0038	0.0007	70.9	9.22	2Q1	0	2.5	0.0011	0.0013	246	76.7
L2	0.0003	560	0.0036	0.0003	61.5	5.32	MK4	0.0004	460	0.0037	0.0003	225	6.12	Q1	0	2.4	0.0010	0.0013	341	157
MK4	0.0003	1600	0.0033	0.0002	224	3.17	MSM	0.0004	1.3	0.0036	0.0063	164	145	MK3	0	1.8	0.0008	0.0011	283	87
M3	0.0003	2100	0.0032	0.0001	179	2.57	MSF	0.0003	0.9	0.0030	0.0061	188	175	J1	0	1.5	0.0008	0.0012	117	106
S1	0.0002	550	0.0027	0.0002	318	5.48	M3	0.0003	320	0.0029	0.0003	180	5.28	3MK7	0	5.4	0.0007	0.0006	253	43.9
H1	0.0002	250	0.0027	0.0003	261	8.39	ETA2	0.0002	57	0.0027	0.0007	102	14.4	M6	0	14	0.0007	0.0004	311	33.2
MSF	0.0001	1.4	0.0022	0.0036	89	98.8	OO1	0.0002	130	0.0027	0.0005	209	9.2	2SK5	0	3.6	0.0006	0.0006	165	61.8
MM	0.0001	1.9	0.0020	0.0029	333	190	NO1	0.0002	130	0.0026	0.0004	139	10.1	SK3	0	1.2	0.0005	0.0009	182	130
NO1	0.0001	190	0.0019	0.0003	119	8.32	Q1	0.0002	230	0.0025	0.0003	147	9.99	2MK5	0	1.9	0.0004	0.0005	112	87.4
SN4	0.0001	420	0.0019	0.0002	181	5.19	MKS2	0.0002	54	0.0024	0.0006	328	18	M8	0	6.8	0.0003	0.0003	33.2	44.1
PI1	0.0001	220	0.0019	0.0002	133	7.71	THE1	0.0001	110	0.0022	0.0004	172	10.9	2MS6	0	3.8	0.0003	0.0003	80.3	62
Q1	0.0001	98	0.0016	0.0003	129	7.25	LDA2	0.0001	44	0.0021	0.0006	51.7	18.8	2SM6	0	2.4	0.0003	0.0003	277	87.8
PSI1	0.0001	130	0.0016	0.0003	282	9.16	J1	0.0001	78	0.0018	0.0004	162	12.5	2MN6	0	1.8	0.0002	0.0002	154	117
MKS2	0.0001	70	0.0015	0.0004	21.9	10.9	SN4	0.0001	79	0.0017	0.0004	185	13.9			**Total A**	**0.386**			
GAM2	0.0001	63	0.0014	0.0003	357	22	MO3	0.0001	120	0.0014	0.0003	285	13.3			**A > 0.001**	**0.381**			
MSM	0	0.7	0.0013	0.0030	72.4	196	SO1	0.0001	36	0.0014	0.0005	19.1	19.5			**% A > 0.001**	**98.57**			
LDA2	0	57	0.0013	0.0003	94.7	14.4	2Q1	0	30	0.0012	0.0004	159	18.7							
ETA2	0	53	0.0012	0.0003	82.5	16.9	BET1	0	33	0.0011	0.0004	309	21	Rmin = 1.00	MinSNR = 1.00	(* SNR >= MinSNR)				
S4	0	150	0.0012	0.0002	98.4	8.99	S4	0	33	0.0011	0.0004	95.9	18.8	K = 4.35	SNRallc = 4.49e + 05					
R2	0	35	0.0010	0.0003	117	18.5	RHO1	0	25	0.0010	0.0004	344	27.9	TVallc = 0.0192	TVsnrc = 0.0192	TVraw = 0.0198				
H2	0	38	0.0009	0.0003	266	20.9	SIG1	0	18	0.0010	0.0004	110	25.3	**PTVallc = 96.8%**	**PTVsnrc = 96.8%**					

(*continued on next page*)

Table 1
(*Continued*)

Sea tide results for 3.7 years							Sea tide results for 1 year							Sea tide results for 1 month						
NAME	PE	SNR	A	A_ci	Ph	Ph_ci	NAME	PE	SNR	A	A_ci	Ph	Ph_ci	NAME	PE	SNR	A	A_ci	Ph	Ph_ci
2Q1	0	57	0.0009	0.0002	184	16.5	MSN2	0	7.6	0.0009	0.0007	267	35.5							
PHI1	0	61	0.0009	0.0002	184	15.4	EPS2	0	7.4	0.0009	0.0006	319	45.2							
EPS2	0	29	0.0009	0.0003	331	22.8	SK3	0	42	0.0009	0.0003	103	18.2							
SK4	0	89	0.0009	0.0002	89.5	12.3	MK3	0	35	0.0008	0.0003	247	22.2							
SK3	0	120	0.0008	0.0001	104	10.9	PHI1	0	12	0.0008	0.0004	219	33.6							
J1	0	28	0.0008	0.0003	174	18.5	CHI1	0	14	0.0007	0.0004	287	31.5							
THE1	0	28	0.0007	0.0003	150	18.9	UPS1	0	8.3	0.0006	0.0004	169	35.2							
MSN2	0	13	0.0007	0.0004	293	27.6	OQ2	0	3.6	0.0006	0.0006	322	79							
MO3	0	79	0.0007	0.0001	277	11.1	TAU1	0	6.3	0.0005	0.0004	80.4	43							
OO1	0	22	0.0006	0.0003	164	24.9	SK4	0	6.3	0.0005	0.0004	85.9	41.2							
SIG1	0	22	0.0006	0.0002	313	26.4	MSK6	0	45	0.0003	0.0001	276	16.5							
OQ2	0	11	0.0006	0.0003	1.76	64.6	2SK5	0	22	0.0003	0.0001	11.2	24.7							
BET1	0	21	0.0006	0.0002	46.2	23.9	2MS6	0	29	0.0003	0.0001	359	49.4							
SO3	0	38	0.0004	0.0001	238	22.3	SO3	0	3	0.0003	0.0003	350	157							
MK3	0	24	0.0004	0.0001	192	24.6	3MK7	0	9.9	0.0002	0.0001	91.3	36.9							
TAU1	0	4.7	0.0003	0.0002	328	47.6	ALP1	0	1.4	0.0002	0.0003	232	128							
2MK5	0	66	0.0003	0.0001	163	11.2	2SM6	0	17	0.0002	0.0001	351	28							
UPS1	0	3.6	0.0002	0.0002	79.6	70	2MK5	0	7.9	0.0001	0.0001	227	50							
M6	0	57	0.0002	0.0001	293	13.2	M6	0	5.8	0.0001	0.0001	352	59.3							
2SK5	0	39	0.0002	0.0001	18.3	19.8	2MK6	0	7.1	0.0001	0.0001	218	46							
MSK6	0	68	0.0002	0.0000	18.9	15.3	2MN6	0	3	0.0001	0.0001	42.8	59.7							
2MN6	0	42	0.0002	0.0000	250	16.4	M8	0	2.9	0.0000	0.0000	307	72.1							
CHI1	0	43	0.0002	0.0002	165	98.3			**Total A**	**0.508**										
2MS6	0	2.2	0.0002	0.0000	7.16	20.9			**A > 0.001**	**0.498**										
ALP1	0	2.1	0.0001	0.0002	117	92.1			**% A > 0.001**	**97.96**										
2SM6	0	31	0.0001	0.0000	346	22.1														
RHO1	0	1.3	0.0001	0.0002	41.6	181	Rmin = 1.00	MinSNR = 1.00	(* SNR >= MinSNR)											
2MK6	0	12	0.0001	0.0001	33.5	31.5	K = 2.26	SNRallc = 7.11e + 05												
3MK7	0	5.9	0.0001	0.0001	191	57	TVallc = 0.0174	TVsnrc = 0.017	TVraw = 0.023											
SO1	0	0.37	0.0001	0.0002	322	193	**PTVallc = 76.5%**	**PTVsnrc = 76.5%**												
M8	0	2.6	0.0000	0.0000	176	58.2														
		Total A	**0.539**																	
		A > 0.001	**0.526**																	
		% A > 0.001	**97.46**																	
Rmin = 1.00	MinSNR = 1.00	(*SNR >= MinSNR)																		
K = 1.80	SNRallc = 2.95e + 06																			
TVallc = 0.0190	TVsnrc = 0.0190	TVraw = 0.0244																		
PTVallc = 77.7%	**PTVsnrc = 77.7%**																			

(*continued on next page*)

Table 1
(*Continued*)

P1 results for 3.7 years							P1 results for 1 year							P1 results for 1 month						
NAME	PE	SNR	A	A_ci	Ph	Ph_ci	NAME	PE	SNR	A	A_ci	Ph	Ph_ci	NAME	PE	SNR	A	A_ci	Ph	Ph_ci
SA	0.4459	1000	0.0764	0.0047	59.7	3	SSA	0.4643	54	0.0570	0.0152	111	13.8	M2	0.7218	4300	0.0511	0.0015	126	1.9
SSA	0.2842	1100	0.0610	0.0037	149	3.76	M2	0.3888	160,000	0.0522	0.0003	70.2	0.303	S2	0.0931	390	0.0184	0.0018	150	4.96
M2	0.2071	70,000	0.0521	0.0004	114	0.484	S2	0.0357	10,000	0.0158	0.0003	74.8	0.963	MSF	0.0719	21	0.0161	0.0068	250	21.5
S2	0.0199	5400	0.0161	0.0004	123	1.36	MSM	0.0295	3.3	0.0144	0.0155	127	63	K1	0.0323	890	0.0108	0.0007	206	3.75
K1	0.0115	15,000	0.0123	0.0002	189	1.11	K1	0.0219	5300	0.0124	0.0003	165	1.71	N2	0.0264	85	0.0098	0.0021	104	10.3
N2	0.0079	2300	0.0101	0.0004	98.7	2.47	MM	0.0186	2.7	0.0114	0.0136	162	70.4	O1	0.0235	540	0.0092	0.0008	158	4.26
MSM	0.0064	19	0.0091	0.0041	277	24.6	N2	0.0141	5700	0.0099	0.0003	53.3	1.62	M4	0.0064	76	0.0048	0.0011	313	13.1
O1	0.005	7400	0.0081	0.0002	163	1.38	O1	0.011	2300	0.0088	0.0004	140	2.59	MS4	0.0059	74	0.0046	0.0011	10.7	13.8
K2	0.0022	490	0.0054	0.0005	133	4.55	K2	0.0046	1800	0.0057	0.0003	79.7	2.78	OO1	0.0056	150	0.0045	0.0007	162	10.4
MM	0.0019	6.9	0.0050	0.0037	159	46.8	MF	0.0034	0.53	0.0049	0.0131	43.4	250	2Q1	0.002	42	0.0027	0.0008	254	13.9
MSF	0.0016	6.7	0.0046	0.0035	204	54.4	P1	0.0021	500	0.0038	0.0003	160	5.61	NO1	0.0018	64	0.0025	0.0006	243	19
P1	0.0013	1200	0.0041	0.0002	188	2.74	MSF	0.0016	0.33	0.0034	0.0114	321	291	MO3	0.0012	25	0.0021	0.0008	172	20.9
H1	0.001	280	0.0036	0.0004	303	6.42	NU2	0.0007	250	0.0022	0.0003	53.5	5.98	J1	0.0011	26	0.0020	0.0008	336	18.7
MF	0.0008	3.7	0.0033	0.0034	62.1	82.5	UPS1	0.0005	95	0.0018	0.0004	184	11.6	SK3	0.0009	27	0.0018	0.0007	218	23.9
GAM2	0.0006	160	0.0028	0.0004	73	9.34	2N2	0.0003	140	0.0016	0.0003	34.2	9.77	MN4	0.0009	9.4	0.0018	0.0012	266	33.1
S1	0.0005	570	0.0026	0.0002	236	3.9	THE1	0.0003	58	0.0016	0.0004	146	14.1	ETA2	0.0009	4.4	0.0018	0.0017	25.6	59.3
H2	0.0003	94	0.0021	0.0004	287	10.4	S4	0.0003	1300	0.0015	0.0001	212	3.15	MK3	0.0008	20	0.0018	0.0008	323	23.5
NU2	0.0003	85	0.0021	0.0004	118	11.9	MU2	0.0003	130	0.0015	0.0003	25.4	10.5	M3	0.0008	19	0.0017	0.0008	273	25.6
MU2	0.0003	72	0.0019	0.0004	73.2	13	CHI1	0.0003	53	0.0014	0.0004	5.42	17.8	Q1	0.0005	17	0.0014	0.0007	140	30.4
2N2	0.0002	59	0.0017	0.0004	79.6	15.4	SK3	0.0003	140	0.0013	0.0002	112	8.11	2MS6	0.0005	24	0.0013	0.0005	175	24.7
T2	0.0002	47	0.0015	0.0004	143	15.4	Q1	0.0002	45	0.0012	0.0004	195	18.5	2MK5	0.0005	7	0.0013	0.0010	23.1	41.3
S4	0.0002	7700	0.0015	0.0000	158	1.23	J1	0.0002	24	0.0011	0.0004	162	19	2SK5	0.0005	7.6	0.0013	0.0009	256	37.4
PI1	0.0001	160	0.0013	0.0002	139	10	SO1	0.0002	26	0.0010	0.0004	65.4	19.1	2MN6	0.0003	13	0.0011	0.0006	359	91.6
R2	0.0001	21	0.0009	0.0004	158	25.6	L2	0.0001	47	0.0009	0.0003	90.8	16.8	2SM6	0.0002	11	0.0009	0.0005	315	37
PSI1	0.0001	86	0.0009	0.0002	258	12.5	NO1	0.0001	25	0.0008	0.0003	142	20.8	UPS1	0.0002	6.6	0.0009	0.0007	213	38.4
NO1	0.0001	64	0.0009	0.0002	146	15.5	2Q1	0.0001	22	0.0008	0.0003	237	25.3	S4	0.0001	1.5	0.0006	0.0010	122	116
UPS1	0.0001	69	0.0008	0.0002	273	13.9	BET1	0.0001	22	0.0008	0.0003	4.14	56.1	M6	0	2.4	0.0004	0.0004	130	101
OO1	0	55	0.0008	0.0002	177	15.9	TAU1	0.0001	16	0.0007	0.0004	217	24.1	3MK7	0	2.2	0.0002	0.0003	325	148
LDA2	0	9.9	0.0007	0.0004	120	33.4	PHI1	0.0001	11	0.0006	0.0004	158	27.7	M8	0	13	0.0002	0.0001	216	33.4
MKS2	0	8.2	0.0006	0.0004	215	40.9	ALP1	0	11	0.0006	0.0003	237	35.9			**Total A**	**0.157**			
2Q1	0	38	0.0006	0.0002	329	19.7	SIG1	0	12	0.0006	0.0003	253	32.2			**A > 0.001**	**0.154**			
L2	0	6.3	0.0006	0.0005	139	40.7	ETA2	0	17	0.0006	0.0003	52.6	25.2			**% A > 0.001**	**98.01**			
M3	0	150	0.0006	0.0001	274	9	MK3	0	23	0.0005	0.0002	245	21.8							
J1	0	29	0.0006	0.0002	218	19.3	M3	0	22	0.0004	0.0002	221	25.6	Rmin = 1.00	MinSNR = 1.00	(* SNR >= MinSNR)				
SIG1	0	26	0.0005	0.0002	288	23.5	SO3	0	12	0.0004	0.0002	68.7	35.6	K = 4.35	SNRallc = 4.40e + 03					
PHI1	0	28	0.0005	0.0002	226	22.6	OO1	0	3.7	0.0003	0.0004	188	58	TVallc = 0.00179	TVsnrc = 0.00179	TVraw = 0.00207				
SO1	0	26	0.0005	0.0002	127	20.1	LDA2	0	5.4	0.0003	0.0003	49.4	45.8	**PTVallc = 86.5%**	**PTVsnrc = 86.5%**					

(*continued on next page*)

Table 1 (*continued*)

P1 results for 3.7 years							P1 results for 1 year							P1 results for 1 month						
NAME	PE	SNR	A	A_ci	Ph	Ph_ci	NAME	PE	SNR	A	A_ci	Ph	Ph_ci	NAME	PE	SNR	A	A_ci	Ph	Ph_ci
EPS2	0	5	0.0005	0.0004	135	57.4	MO3	0	12	0.0003	0.0002	283	33.2							
TAU1	0	14	0.0004	0.0002	355	71.1	EPS2	0	4	0.0003	0.0003	3.73	220							
BET1	0	14	0.0004	0.0002	61.6	29.8	MN4	0	10	0.0002	0.0001	151	32.8							
SK3	0	51	0.0004	0.0001	82.5	12.8	M4	0	7.5	0.0001	0.0001	163	35							
Q1	0	17	0.0004	0.0002	177	30.8	MK4	0	12	0.0001	0.0001	340	40.2							
OQ2	0	3.5	0.0003	0.0004	188	69.9	MSN2	0	1.5	0.0001	0.0002	80	153							
RHO1	0	7.2	0.0003	0.0002	133	36.7	MKS2	0	0.88	0.0001	0.0002	231	104							
ETA2	0	1.9	0.0003	0.0004	72.4	76.4	SN4	0	4.2	0.0001	0.0001	228	62.2							
ALP1	0	6.4	0.0003	0.0002	290	41.5	OQ2	0	0.8	0.0001	0.0002	287	170							
MSN2	0	2	0.0002	0.0003	165	110	RHO1	0	0.31	0.0001	0.0002	26.3	281							
M4	0	160	0.0002	0.0000	270	7.83	2MK6	0	340	0.0001	0.0000	296	5.51							
SO3	0	9.4	0.0001	0.0001	68.2	42.1	2MK5	0	120	0.0000	0.0000	81.8	9.41							
CHI1	0	2.4	0.0001	0.0002	15.7	228	MSK6	0	270	0.0000	0.0000	349	8.5							
MS4	0	38	0.0001	0.0000	312	14.6	SK4	0	1.5	0.0000	0.0001	143	118							
THE1	0	1.8	0.0001	0.0002	167	95.2	2MS6	0	140	0.0000	0.0000	49.8	9.5							
MN4	0	43	0.0001	0.0000	245	20	2SM6	0	160	0.0000	0.0000	98.7	8.93							
MK4	0	23	0.0001	0.0000	317	25.7	MS4	0	1.3	0.0000	0.0001	40.8	163							
SN4	0	9.5	0.0001	0.0000	242	41.3	2MN6	0	100	0.0000	0.0000	72.4	10.8							
MO3	0	1.5	0.0000	0.0001	163	123	2SK5	0	39	0.0000	0.0000	227	17.7							
MK3	0	1.3	0.0000	0.0001	91.6	138	M6	0	43	0.0000	0.0000	331	18.3							
2SK5	0	190	0.0000	0.0000	0.878	23.5	3MK7	0	140	0.0000	0.0000	2.43	12.2							
MSK6	0	220	0.0000	0.0000	346	7.81	M8	0	16	0.0000	0.0000	182	32.7							
SK4	0	2.4	0.0000	0.0000	70.4	96.9			**Total A**	**0.226**										
2MN6	0	100	0.0000	0.0000	6.18	13.9			**A > 0.001**	**0.216**										
2MS6	0	61	0.0000	0.0000	122	17.2			**% A > 0.001**	**95.43**										
3MK7	0	660	0.0000	0.0000	266	5.96			**Total A**	**0.226**										
2MK6	0	28	0.0000	0.0000	209	19.2	Rmin = 1.00	MinSNR = 1.00	(* SNR >= MinSNR)											
M8	0	32	0.0000	0.0000	170	20.9	K = 2.26	SNRallc = 3.13e + 03												
M6	0	27	0.0000	0.0000	350	29.7	TVallc = 0.00353	TVsnrc = 0.00351	TVraw = 0.0155											
2MK5	0	19	0.0000	0.0000	30.4	24.7	**PTVallc = 22.8%**	**PTVsnrc = 22.7%**												
2SM6	0	2.6	0.0000	0.0000	267	79.3														
		Total A	**0.303**																	
		A > 0.001	**0.289**																	
		% A > 0.001	**95.31**																	
Rmin = 1.00	MinSNR = 1.00	(* SNR >= MinSNR)																		
K = 1.80	SNRallc = 5.52e + 03																			
TVallc = 0.00612	TVsnrc = 0.00612	TVraw = 0.0450																		
PTVallc = 13.6%	PTVsnrc = 13.6%																			

(*continued on next page*)

Table 1
(*Continued*).

P2 results for 3.7 years							P2 results for 1 year							P2 results for 1 month						
NAME	PE	SNR	A	A_ci	Ph	Ph_ci	NAME	PE	SNR	A	A_ci	Ph	Ph_ci	NAME	PE	SNR	A	A_ci	Ph	Ph_ci
SA	0.6619	1100	0.0676	0.0040	46.5	3.64	SSA	0.7939	77	0.0465	0.0104	119	12.4	M2	0.4535	4600	0.0183	0.0005	123	1.7
SSA	0.2612	310	0.0425	0.0047	142	6.12	M2	0.1211	120,000	0.0182	0.0001	68.2	0.411	MSF	0.4503	27	0.0182	0.0069	272	24.8
M2	0.05	35,000	0.0186	0.0002	113	0.518	MSM	0.0298	4.5	0.0090	0.0083	173	74.5	S2	0.0342	330	0.0050	0.0005	93.2	5.83
MSM	0.0113	16	0.0089	0.0044	215	27.9	MF	0.0175	2.3	0.0069	0.0090	21	140	N2	0.0182	180	0.0037	0.0005	96.9	8.6
MM	0.005	7.5	0.0059	0.0042	195	41.5	MSF	0.0085	1.5	0.0048	0.0078	296	130	OO1	0.0121	180	0.0030	0.0004	87.9	7.89
S2	0.0032	2600	0.0047	0.0002	69.3	2.51	S2	0.0085	8200	0.0048	0.0001	16	1.31	J1	0.0093	150	0.0026	0.0004	23.1	7.7
N2	0.0019	900	0.0036	0.0002	98.6	3.17	MM	0.0058	1.2	0.0040	0.0072	89.8	137	O1	0.0043	55	0.0018	0.0005	192	13.3
K1	0.0016	2700	0.0034	0.0001	187	2.35	N2	0.0048	4400	0.0036	0.0001	51.4	1.8	M4	0.0034	120	0.0016	0.0003	295	10.9
O1	0.0011	2500	0.0027	0.0001	164	2.54	K1	0.0028	610	0.0028	0.0002	164	4.59	NO1	0.0026	39	0.0014	0.0004	278	15.6
S1	0.0006	960	0.0020	0.0001	186	3.3	O1	0.0028	590	0.0027	0.0002	147	4.65	K1	0.0026	53	0.0014	0.0004	125	15.5
MF	0.0005	1.1	0.0019	0.0036	40.8	183	K2	0.0009	760	0.0015	0.0001	69.8	4	2Q1	0.0023	34	0.0013	0.0004	247	18.4
K2	0.0004	220	0.0016	0.0002	130	6.42	SK3	0.0006	530	0.0013	0.0001	115	4.51	SK3	0.0019	130	0.0012	0.0002	231	12
MSF	0.0002	0.57	0.0011	0.0027	293	206	P1	0.0006	130	0.0012	0.0002	174	9.54	ETA2	0.0017	19	0.0011	0.0005	120	27.5
H2	0.0002	95	0.0011	0.0002	303	11.3	NO1	0.0004	71	0.0010	0.0002	118	13.1	MS4	0.001	39	0.0009	0.0003	353	25.6
T2	0.0001	79	0.0008	0.0002	268	12.5	2N2	0.0002	150	0.0008	0.0001	33.4	10.4	2SK5	0.0007	48	0.0007	0.0002	125	13.1
NU2	0.0001	75	0.0008	0.0002	121	13.2	2Q1	0.0002	40	0.0008	0.0002	255	16.9	MN4	0.0004	15	0.0005	0.0003	248	31.1
H1	0.0001	70	0.0008	0.0002	64	12.7	NU2	0.0002	140	0.0007	0.0001	57.4	8.86	Q1	0.0004	7.3	0.0005	0.0004	99.7	45.4
PI1	0.0001	100	0.0007	0.0001	108	11.7	OO1	0.0002	37	0.0007	0.0002	109	20.4	UPS1	0.0003	5.3	0.0005	0.0004	12.6	67.2
P1	0.0001	87	0.0006	0.0001	226	10.1	UPS1	0.0001	33	0.0006	0.0002	125	17.2	2MK5	0.0002	14	0.0004	0.0002	281	21.1
Q1	0.0001	73	0.0006	0.0001	172	11.3	BET1	0.0001	24	0.0006	0.0002	346	22.6	2MS6	0.0002	52	0.0004	0.0001	128	19.8
2N2	0.0001	40	0.0006	0.0002	82.1	17.9	CHI1	0.0001	23	0.0006	0.0002	23.5	22.2	S4	0.0002	6.3	0.0003	0.0003	216	45.2
SK3	0.0001	520	0.0006	0.0001	124	4.56	Q1	0.0001	29	0.0005	0.0002	205	23.5	MK3	0.0001	7.6	0.0003	0.0002	14.5	52.1
R2	0	25	0.0005	0.0002	112	19.7	MU2	0.0001	70	0.0005	0.0001	51.5	13.1	2SM6	0	12	0.0002	0.0001	358	95.7
2Q1	0	46	0.0005	0.0001	327	15.4	L2	0.0001	62	0.0005	0.0001	77.7	13	2MN6	0	10	0.0002	0.0001	301	36.4
PSI1	0	52	0.0005	0.0001	215	14.5	S4	0.0001	980	0.0005	0.0000	263	3.24	MO3	0	1.9	0.0001	0.0002	12.6	202
MU2	0	23	0.0005	0.0002	55.9	24	MKS2	0.0001	67	0.0005	0.0001	8.13	14.7	3MK7	0	6.7	0.0001	0.0001	241	54.6
S4	0	2700	0.0004	0.0000	215	2.19	TAU1	0.0001	18	0.0004	0.0002	218	32.8	M6	0	3.2	0.0001	0.0001	324	103
MKS2	0	14	0.0004	0.0002	230	27.4	THE1	0.0001	13	0.0004	0.0002	154	34.7	M3	0	0.81	0.0001	0.0002	27.2	231
M3	0	120	0.0003	0.0001	280	10.3	EPS2	0.0001	69	0.0004	0.0001	63.9	17.8	M8	0	9.3	0.0000	0.0000	247	44.4
GAM2	0	10	0.0003	0.0002	214	35.6	MSN2	0	47	0.0004	0.0001	105	14.6			**Total A**	**0.066**			
ETA2	0	9.5	0.0003	0.0002	41	40.6	RHO1	0	6.1	0.0003	0.0003	41	40.2			**A>0.001**	**0.061**			
OO1	0	17	0.0003	0.0001	55.6	29.4	SIG1	0	12	0.0003	0.0002	181	35			**% A>0.001**	**91.84**			
J1	0	19	0.0003	0.0001	202	28.6	J1	0	9.5	0.0003	0.0002	130	38.1			**Total A**	**0.066**			
NO1	0	20	0.0003	0.0001	192	29.4	SO1	0	5.7	0.0003	0.0003	75.7	40	Rmin= 1.00	MinSNR= 1.00	(* SNR >= MinSNR)				
L2	0	6.5	0.0002	0.0002	150	39.4	PHI1	0	8.2	0.0003	0.0002	115	44.9	K= 4.35	SNRallc= 804					
UPS1	0	14	0.0002	0.0001	267	34.9	M3	0	27	0.0003	0.0001	184	20.9	TVallc= 0.000372	TVsnrc= 0.000372	TVraw= 0.000779				
LDA2	0	5.4	0.0002	0.0002	74.8	49	ALP1	0	3.3	0.0002	0.0002	220	60.7	**PTVallc= 47.7%**	**PTVsnrc= 47.7%**					

(*continued on next page*)

Table 1 (*continued*)

P2 results for 3.7 years							P2 results for 1 year							P2 results for 1 month						
NAME	PE	SNR	A	A_ci	Ph	Ph_ci	NAME	PE	SNR	A	A_ci	Ph	Ph_ci	NAME	PE	SNR	A	A_ci	Ph	Ph_ci
THE1	0	9	0.0002	0.0001	240	40.7	MO3	0	13	0.0002	0.0001	310	31.7							
SO1	0	7.4	0.0002	0.0001	66.2	41.9	MK3	0	8.6	0.0002	0.0001	180	37.9							
MO3	0	48	0.0002	0.0001	47.5	16.4	OQ2	0	5	0.0001	0.0001	97.5	43.4							
SIG1	0	8.1	0.0002	0.0001	25	41.6	LDA2	0	3.9	0.0001	0.0001	82.7	57.8							
OQ2	0	3.7	0.0002	0.0002	206	61.8	MN4	0	43	0.0001	0.0000	115	15.8							
RHO1	0	5.9	0.0002	0.0001	154	38.7	SK4	0	25	0.0001	0.0000	169	20.9							
PHI1	0	5.6	0.0002	0.0001	264	46.7	ETA2	0	1.7	0.0001	0.0001	141	84.7							
SO3	0	36	0.0001	0.0000	37.5	19.1	MK4	0	17	0.0001	0.0000	310	32.7							
BET1	0	3.6	0.0001	0.0001	223	53.7	M4	0	19	0.0001	0.0000	117	30.3							
CHI1	0	3.3	0.0001	0.0001	268	75	2MK5	0	510	0.0000	0.0000	90.2	4.73							
ALP1	0	2.7	0.0001	0.0001	337	95.2	2MK6	0	790	0.0000	0.0000	268	4.69							
MSN2	0	2.1	0.0001	0.0001	70.6	117	SO3	0	1.2	0.0000	0.0001	331	225							
MK3	0	18	0.0001	0.0000	187	27.3	SN4	0	6.5	0.0000	0.0000	305	42.8							
TAU1	0	1.3	0.0001	0.0001	240	102	MS4	0	6.4	0.0000	0.0000	103	57.7							
EPS2	0	0.53	0.0001	0.0001	39.3	184	2MS6	0	280	0.0000	0.0000	61.9	6.62							
SK4	0	49	0.0001	0.0000	245	16.6	MSK6	0	240	0.0000	0.0000	323	6.1							
MS4	0	33	0.0000	0.0000	63	20.7	2MN6	0	330	0.0000	0.0000	78.9	6.42							
M4	0	12	0.0000	0.0000	280	34.1	2SM6	0	200	0.0000	0.0000	105	6.59							
SN4	0	9.9	0.0000	0.0000	156	34.9	3MK7	0	900	0.0000	0.0000	12.6	3.07							
MN4	0	4.5	0.0000	0.0000	304	46.6	M6	0	52	0.0000	0.0000	1.42	24.2							
2MK6	0	850	0.0000	0.0000	9.46	3.82	M8	0	24	0.0000	0.0000	163	19.4							
MSK6	0	850	0.0000	0.0000	191	4.64	2SK5	0	0.76	0.0000	0.0000	297	144							
2MN6	0	680	0.0000	0.0000	215	4.57			**Total A**	**0.120**										
M6	0	720	0.0000	0.0000	152	3.7			**A>0.001**	**0.108**										
2SM6	0	640	0.0000	0.0000	74.2	4.53			**% A>0.001**	**89.98**										
3MK7	0	4800	0.0000	0.0000	126	1.66														
MK4	0	2.2	0.0000	0.0000	27.8	119	Rmin = 1.00	MinSNR = 1.00	(* SNR >= MinSNR)											
2MK5	0	290	0.0000	0.0000	225	6.69	K = 4.58	SNRallc = 3.53e + 03												
2MS6	0	100	0.0000	0.0000	309	10.2	TVallc = 0.00137	TVsnrc = 0.00137	TVraw = 0.00687											
M8	0	26	0.0000	0.0000	312	25.1	**PTVallc = 20.0%**	**PTVsnrc = 20.0%**												
2SK5	0	11	0.0000	0.0000	239	31.8														
		Total A	**0.179**																	
		A > 0.001	**0.166**																	
		% A > 0.001	**92.66**																	
Rmin = 1.00	MinSNR = 1.00	(* SNR >= MinSNR																		
K = 4.38	SNRallc = 1.52e + 04																			
TVallc = 0.00316	TVsnrc = 0.00316	TVraw = 0.0212																		
PTVallc = 14.9%	**PTVsnrc = 14.9%**																			

quencies therefore will be better fitted. This fact is due to the lack of detections of the lower frequencies in the shorter time series.

Solar annual (SA) and solar semiannual constituents (SSA) were detected as the main lowest frequencies in the 3.7 year time series for the tide, P1, and P2 monitoring. Conversely, in the one-month time series, the moon-solar fortnightly constituent (MSF) was always the lowest frequency. In the one-year time series, the SA (solar annual) constituent was not detected, and the main constituents therefore were SSA and M2 (solar semiannual and moon semidiurnal). Moreover, the constituent fitted with the highest amplitude at P1 and P2 in the longest time series (3.7 years) was SA, whereas in the tidal records, it was M2. Fig. 4 shows (for the 3.7 year record at P1 and P2) the decouplings in the fitting amplitude at the lower frequencies (mainly the SA, SSA, MM, and MSM constituents) for the tide. This finding highlights the contribution of the non-tidal sources of perturbations such as the recharge processes in the aquifer at both piezometers, and as a consequence the tidal portions of the raw signals in P1 and P2 were not the principal sources of the perturbations when the longer time series were analysed.

The heads showed differences after applying this method using time series lengths of 3.7 years, one year and one month, as shown in Fig. 5. The filtered results for 3.7 years are not shown due to their poor resolution and the difficulty in obtaining an acceptable visualization. For the one-month time series of groundwater head (graphs A-2 and B-2 in Fig. 5), the main tidal constituents (M2, S2, and MSF) were easier to fit and extract than for the longer time series, mainly because the large amount of low-frequency variability in the entire time series hindered the fitting of higher frequencies. Probably as a consequence, the fit of the tidal variance of HA (first block in Table 1A, B, and C) was smaller in the longer analysed time series. Otherwise, the low-tidal frequency data were lost in the one-month analysis due to its absence (or weak presence) in that time series. The fitted tidal part (blue lines in Fig. 5) corresponded to the astronomical extracted component of the tide from the groundwater heads at P1 and P2, and the residual part is considered to be the tide-filtered head. In P1, this tidal influence was clearly higher than in P2. The differences in the amplitude values fitted for each time series length between P1 and P2 reveal the importance of depth in the groundwater measurements, as shown by the values for constituent M2, which varied from 0.156 m in the tide to 0.0521 m in P1 and 0.0186 m in P2 (Table 1A, B and C). This reveals the larger and more rapid sea-aquifer connection at depth in the unconfined aquifer. Likewise, this responds to the change in the storage coefficient through the thickness of the aquifer close to the sea, where a change in pressure near the phreatic surface reflects the movement of higher volumes of water than in the deeper parts of the aquifer, near the bottom of the aquifer, where the storage coefficient seems to be close to the confined values (Erskine, 1991; Nielsen et al., 1997). Otherwise, the difference in the groundwater head levels between P1 and P2 may be explained by the difference in pressure as a consequence of non-hydrostatic pressure (Nielsen, 1990; Wu, 2009). In that regard, this pressure effect is not considered to have affected the tidal extraction processes using the applied methods because the filtering was based on the signal oscillations (amplitude and phase). However, the effect of non-hydrostatic pressure should be considered to determine the absolute groundwater head level at each measured point as a further analysis after the filtering process.

4.2. Fitting and filtering of tidal part with the CWT method

The main frequency bands were fitted depending on the time series length. Diurnal (D1, 24 h), semidiurnal (D2, 12 h), quarter diurnal (D4, 6 h), and occasionally eight diurnal (D8, 3 h) were fitted and extracted from the one-month time series. However, for the one year and the 3.7 year time series, it was also necessary to include additional frequency bands that allowed the lower frequency tidal constituents present in the time series to be fitted and extracted. Those bands were equivalent to the fortnightly constituents (MSF and MF) and the annual and semi-annual constituents (SA and SSA).

Table 2
Maximum relative error (Max. error) and quadratic relative error (L2 error) obtained for each time series length (one month, one year, and 3.7 years) at P1 and P2 relative to the reconstruction of the time series by applying the CWT method, taking into account all the scales defined in the analysis. The reconstructed signal is the sum of the fitted and extracted tidal component and the residual (non-tidal) component.

Relative errors: reconstructed signal by CWT				
Period	P1		P2	
	Max. error	L2 error	Max. error	L2 error
Month	2.05%	1.38%	2.31%	2.20%
Year	2.64%	2.55%	3.84%	2.70%
3.7 years	3.94%	3.08%	3.93%	2.99%

The time-scale analysis of the data for a one-month time series (Fig. 6) shows the inverse relation between scale and the pseudo-frequency bands, where the tidal influence is remarkable. The D2 tide band was recognized in the frequency interval 0.08–0.1 (h^{-1}) (left vertical axis), and the D1 band was recognized in the frequency interval 0.1–0.15 (h^{-1}). A certain degree of overlap was also visible between D1 and D2, as mentioned by Flinchem and Jay (2000), in the complete frequency range of 0.08–0.15 (h^{-1}). That overlap produced an increase or decrease in amplitude in the semidiurnal constituents, which yield spring and neap tides, respectively. In a general sense, the main tidal bands detected for each time series length in P1 and P2 were similar (D1 and D2), but the D1 band was more clearly seen in P1. In addition, the amplitudes differed from each other, and the maximum amplitudes were lower in P1 because they were more influenced by the tide. P2 was more affected by non-tidal forces, as can be best observed in the lower frequencies (Fig. 6).

The lowest-frequency tidal band extracted from the one-month time series was the fortnightly one, which was recognized as the highest amplitudes in bands D1 and D2. In addition, frequency bands D4 and D8 appeared in the frequency fringe above 0.15 (h^{-1}). There were also occasional higher frequencies that constituted noise, especially in P1 (oscillations with periods below 2.5 h), which were also extracted. Thus, the approximate frequencies taken into account to filter the time series were defined for D1 in the range of 0.0357–0.0463 (h^{-1}), for D2 in the range of 0.0734–0.0879 (h^{-1}), and for D4 in the range of 0.1553–0.1697 (h^{-1}). These results are similar to those of Guo et al. (2015), with these bands comprising almost the entirety of the tidal frequencies in one month at both P1 and P2. For one year, the results matched in shape with the one-month results of the frequency bands present in both cases, but new, lower frequencies were detected at lower ranges between 2.5×10^{-3} and 3.2×10^{-3} (h^{-1}). These frequencies allowed the fortnightly and monthly tidal constituents to be fitted. The same process was performed with the 3.7 year time series, and in that case the annual and semi-annual tidal constituents were added to the fit (frequencies of 1.14×10^{-5} and 2.28×10^{-5} (h^{-1}), respectively). The achieved fits (original signal versus reconstructed signal) were evaluated using the maximum and quadratic relative errors, which are shown in Table 2 for each tie series length at both P1 and P2; all of them were below 4% when all the defined scales were taken into account.

Fig. 7 shows the filtered groundwater heads at P1 and P2 for one year (A-1 and B-1) and one month (A-2 and B-2). The fil-

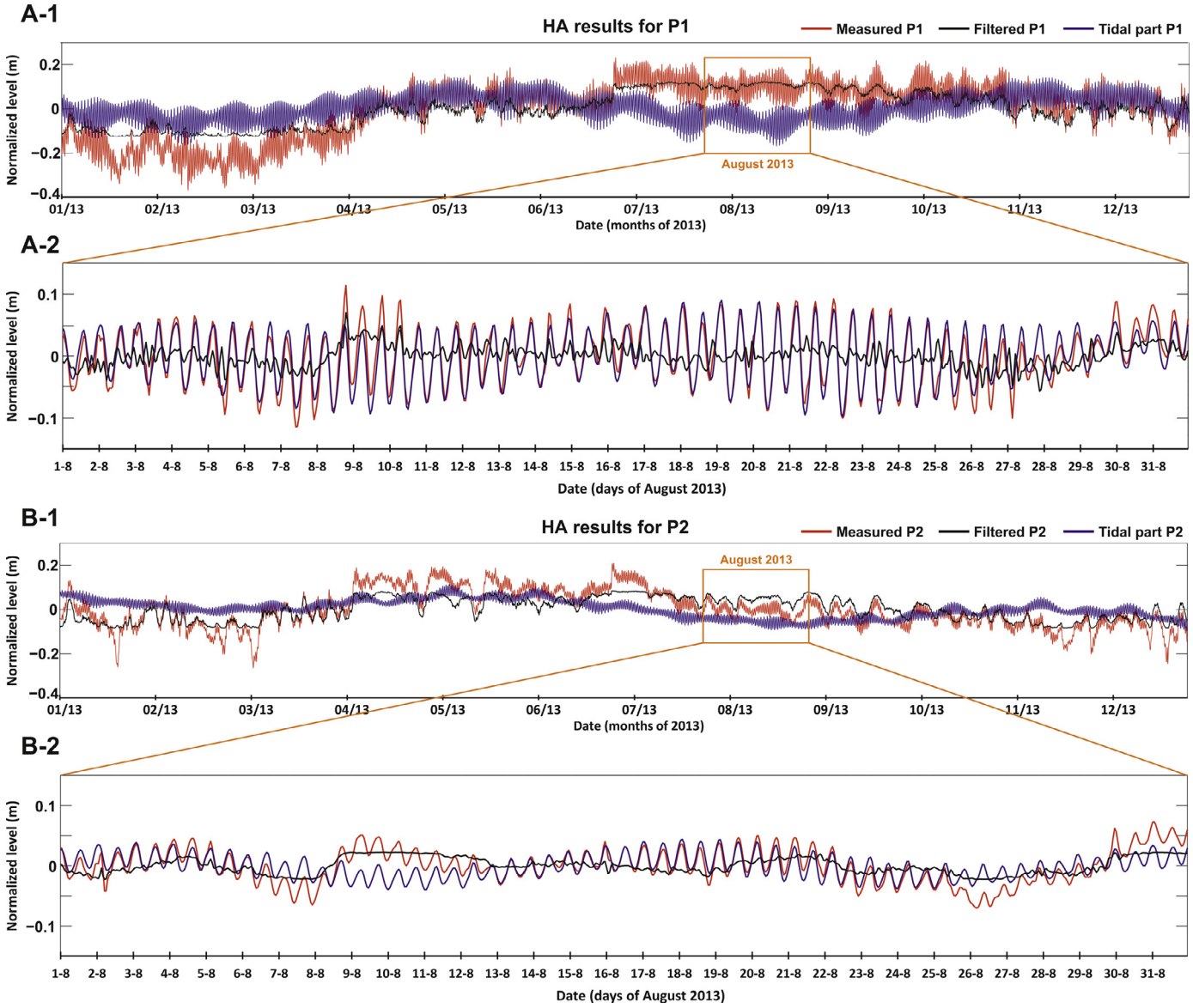

Fig. 5. One-year and one-month results of the HA method from the groundwater heads at P1 (A) and P2 (B). The one-month time series (A-2 and B-2) corresponded to August 2013, which was included in the one-year time series of 2013 (A-1 and B-1), but the method was applied in each time series independently. The measured groundwater heads (red lines) were decomposed in the fitted part due to the tidal effects (blue lines) and residual parts (black lines) at P1 and P2. The filtering was performed separately for each time series. (For interpretation of the references to colour in this figure legend, the reader is referred to the web version of this article.)

tered results for 3.7 years are not shown due to the poor resolution and difficulty in obtaining an acceptable visualization. The black lines correspond to the filtered groundwater heads at P1 and P2 for both time series, whereas the blue lines are the extracted tidal components. All the frequency bands considered led to an almost complete extraction, where the tidal influences at P1 and P2 were completely extracted and the non-tidal part remained.

4.3. Evaluation of the methods

Fig. 8 shows a comparison of the filtered heads for both the P1 and P2 piezometers obtained by the HA and CWT methods for the 3.7 year, one-year and one-month time series. The comparison is centred in the one-month time series, where the three different time series are coincident in time.

The filtered head obtained by the HA method (Fig. 8A and B) showed a residual tidal oscillation for the 3.7-year time series, which corresponded in frequency to the semidiurnal and diurnal constituents. This was more obvious in P1 than in P2, and it had a dampening effect (less remarkable) at the shorter time series. For a month, the major tidal constituents (M2, S2, and MSF) were fitted and filtered. Lower tidal frequencies such as the monthly and semi-annual tidal constituents were not present and hence not fitted and filtered in one month, which produced some differences between these and the one-year results. In the same way, the annual constituent was only filtered in the 3.7 year time series, resulting in some trending differences. In all the time series, some noise remained in the filtered heads.

Summarizing, the filtered results obtained by the CWT method (Fig. 8C and D) yielded a practically complete extraction of the tidal influences in P1 and P2, although they showed few differences between the filtered time series lengths for the lowest frequencies. Conversely, the filtered results obtained by the HA showed a lack of fit for diurnal tidal frequencies when the method is applied in the longer time series. This was verified by the comparison of the standard deviations of the residual tidal oscillations

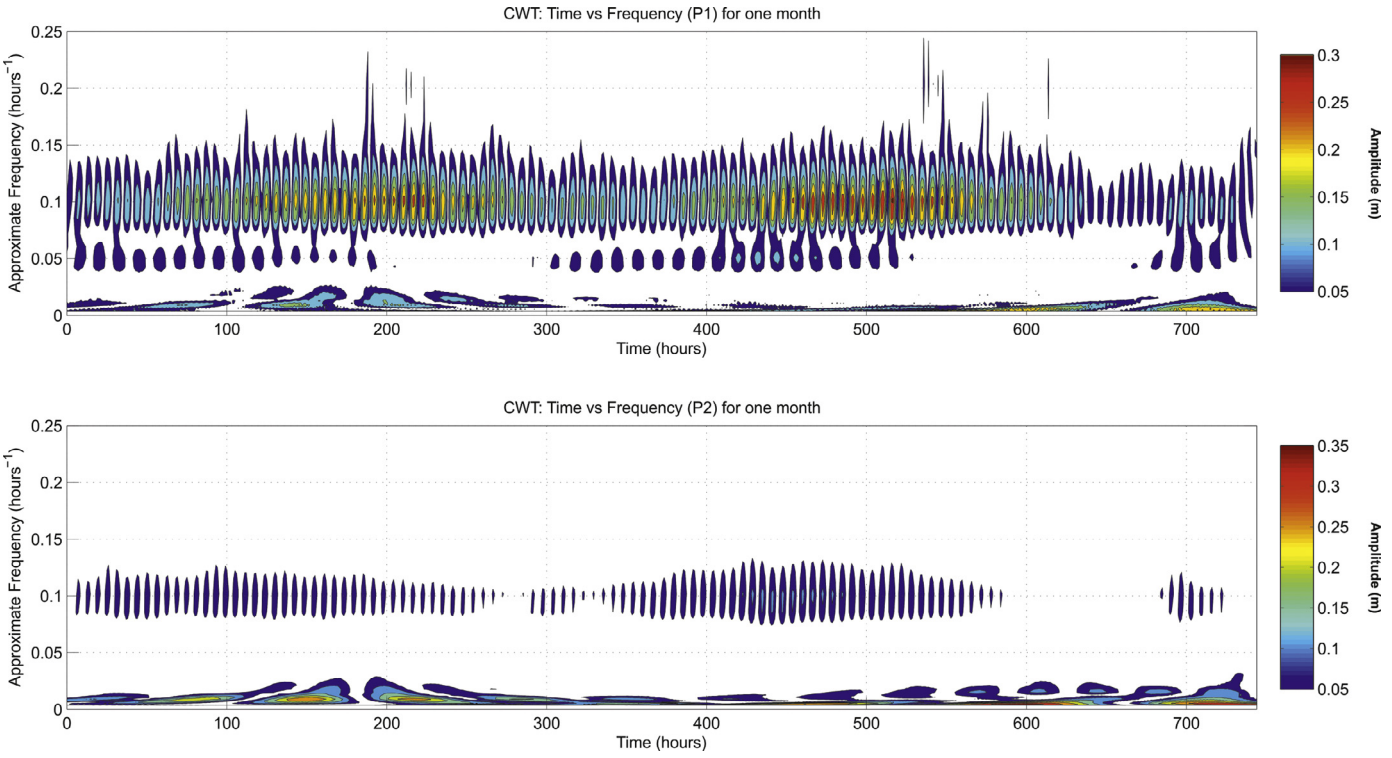

Fig. 6. Time-frequency analysis of the CWT results for P1 (A) and P2 (B) in the one-month time series. The right-hand coloured bar show the variation in amplitude (m) at each considered frequency band (inverse of scales). Note that the values of the colour bar are different for each point, and values below 0.05 m are in white. (For interpretation of the references to colour in this figure legend, the reader is referred to the web version of this article.)

remaining in both methods. The standard deviation with the HA method in the longer time series (3.7 years) was 0.0201 m for P1 and 0.0108 m for P2 while with the CWT method was 0.0024 m for P1 and 0.0025 m for P2.

5. Discussion

The analysed constituents in a signal are first restricted by the number of occurrences of each constituent within the signal, which was verified with both methods. This means that a specific constituent must appear in the analysed time series at least twice its period (two complete oscillations) within the analysed record. Generally, a greater number of oscillations of a given constituent leads to a better definition of it, so that the detection and fit of higher frequencies should be better than at lower frequencies in a determined time series length. Conversely, in this case, when the analysed time series is shorter, the tidal constituents in a record were more easily detected and fitted because the high-frequency tidal portion (diurnal and lower periods) is more significant within the whole signal, and this occurs especially when the HA method is applied. Because of this, the apparent amplitudes of higher-frequency constituents may be incorrectly enhanced or reduced by the amplitudes of the lower-frequency constituents in the shorter time series, which are present but impossible to fit with filtering purposes. A proper filtering of a specific constituent also depends on its similarities with other occasional non-tidal oscillations, which could be close to it in frequency.

The HA fit results for P1 and P2 (Table 1A, B, and C) showed different values of the main tidal constituents for the 3.7 year time series for the constituents found in the tidal level. For the analysed tide, the major constituent (regarding the amplitude) was clearly the semi-diurnal (M2) constituent, whereas for P1 and P2, the major constituents were the solar annual and solar semiannual (SA and SSA) constituents. This could have been caused by the incorrect fitting of the low-frequency tidal oscillations in the groundwater heads, where the low frequencies of the non-tidal sources of the perturbation (e.g., the seasonal recharge oscillations) were partially or fully added to the low-frequency tidal constituents. This effect was greater in P2, where the measured groundwater head showed higher oscillations at the low frequencies than in P1, so that part of the non-tidal forces was fitted as low-frequency tidal oscillations. Therefore, the fitted constituents SA and SSA at P2 were higher than in the sea level and P1 measurements. The amplitude of the oscillation of the non-tidal component (recharge factors of the aquifer and other non-tidal sources) in P2 was higher than in P1, with the non-tidal portion being more prominent in P2 than the tidal component (its tidal influence), as noted in the HA method. By contrast, the higher tidal frequencies in P1 were more noticeable than in P2 because they were better detected and hence better fitted in the deeper parts of the aquifer.

The CWT results suggest that the adjustment in the frequency bands and the resolution between frequencies were better for the longer time series, where the tidal constituents had more oscillations to achieve a better fitting. CWT is useful to maintain the constant time-frequency relation of Eq. (28) because the filtered results of the different analysed time series lengths appeared to be similar with each other. The total fit achieved in each time series length was acceptable, considering the low error values in the comparison of the reconstructed and original time series (Table 2). In cases where the non-tidal processes were still evident in the filtered heads, the CWT method could be useful for further analysis, only considering additional filters that match all the possible detected constituents, but the nature and periodicity of those non-tidal processes must be well known (in terms of frequency and amplitude) to achieve acceptable fits.

The CWT method is a novel type of analysis for groundwater time series and offers good possibilities for development in further tidal and non-tidal studies. The correct recovery of both tidal

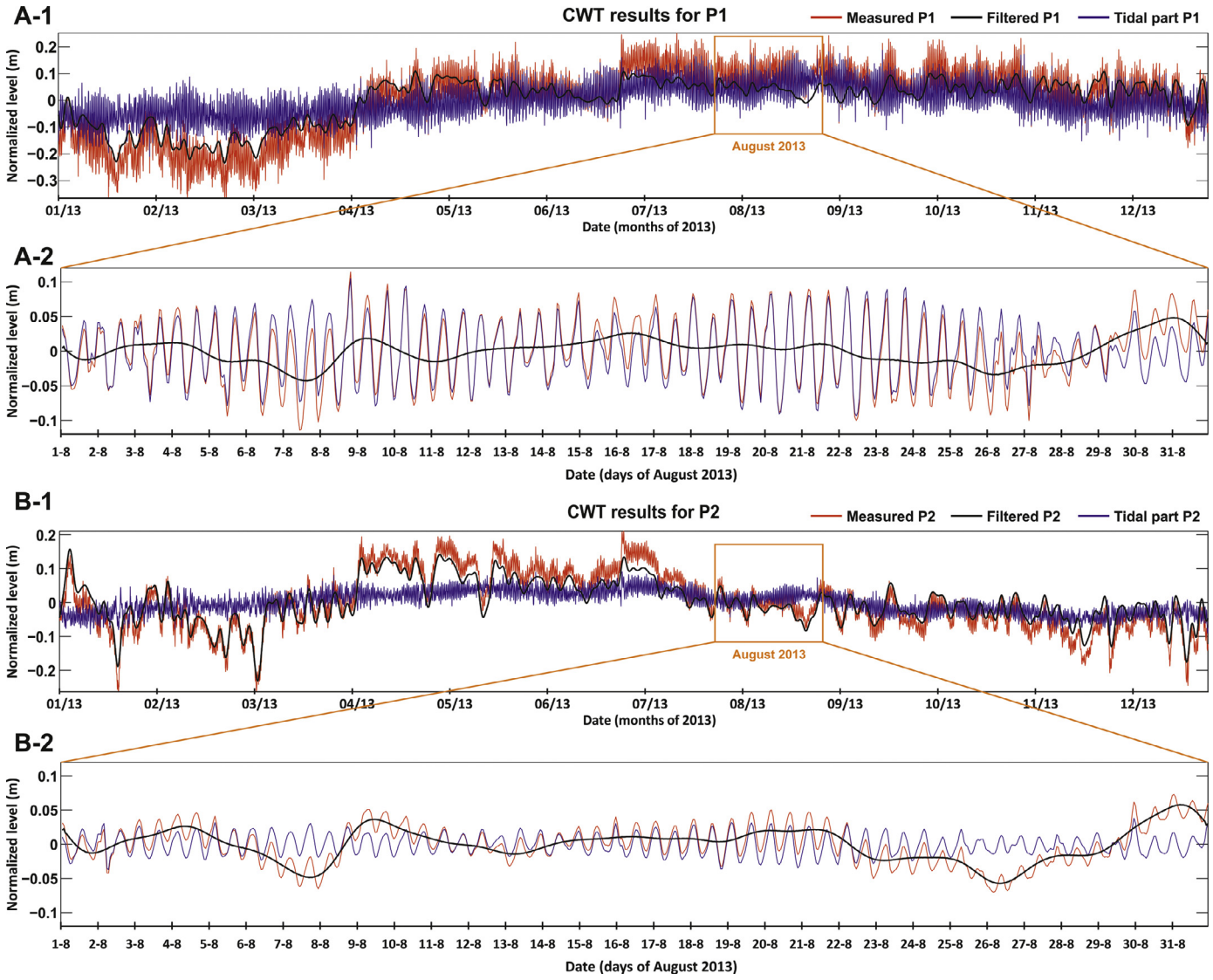

Fig. 7. One-year and one-month results of the CWT method from the groundwater heads at P1 (A) and P2 (B). The one-month time series (A-2 and B-2) corresponded to August 2013, which was included in the one-year time series of 2013 (A-1 and B-1). The measured groundwater heads (red lines) were decomposed in the fitted part due to the tidal effects (blue lines) and residual parts (black lines) at P1 and P2. The filtering was performed separately for each time series. (For interpretation of the references to colour in this figure legend, the reader is referred to the web version of this article.)

and non-tidal components of the groundwater head is determined by the resolution limits set by the Heisenberg restriction. The HA method is also valid for the analysis of tidal influence on groundwater heads, but it is insufficient for the non-tidal part, especially in cases when the non-tidal part of the measurements is higher than the tidal part. Moreover, when HA method was applied in the longest time series (3.7 years), a residual oscillation was observed of the semidiurnal and diurnal tidal oscillations in the filtered signal, with a standard deviation of 0.0201 m for these residuals, compared with 0.0024 m with the CWT method at P1, and 0.0108 m (HA) and 0.0025 m (CWT) at P2. For one year and one month, this lack of fit had a standard deviation lower than 1×10^{-3} m.

The inland recharge processes produce the behaviour of the groundwater head throughout the aquifer system, but this cannot be recognized in tidal-influenced coastal regions without removing those tidal effects from the time series, especially when the non-tidal oscillations in the analysed dataset are close in frequency to the tidal oscillations and when the tidal frequency band is overly wide.

Teo et al. (2003) noted that the non-linear component of the tide-induced groundwater variation plays an important role. Likewise, the higher-order correction of the linear solution is expected to be particularly important under certain combinations of wave and soil characteristics in coastal aquifers (due to high-frequency tidal oscillations or waves in shallow waters). The non-linear components due to tides were neglected in this study because the features of the aquifer and sea-aquifer configuration do not yield perceptible non-linear perturbations. Nonetheless, the non-linear behaviour of the groundwater head should be considered in further studies where the inland processes that may control this non-tidal behaviour are monitored. Otherwise, the influence of groundwater over-height may contribute to the non-tidal part. The features of the aquifer and the sea-aquifer configuration in this case could have caused the verified negligible effect of the over-height in the groundwater heads at P1 and P2 (distance from the shore and depth) but should be considered when factors that indicate a significant influence of over-height are recognized.

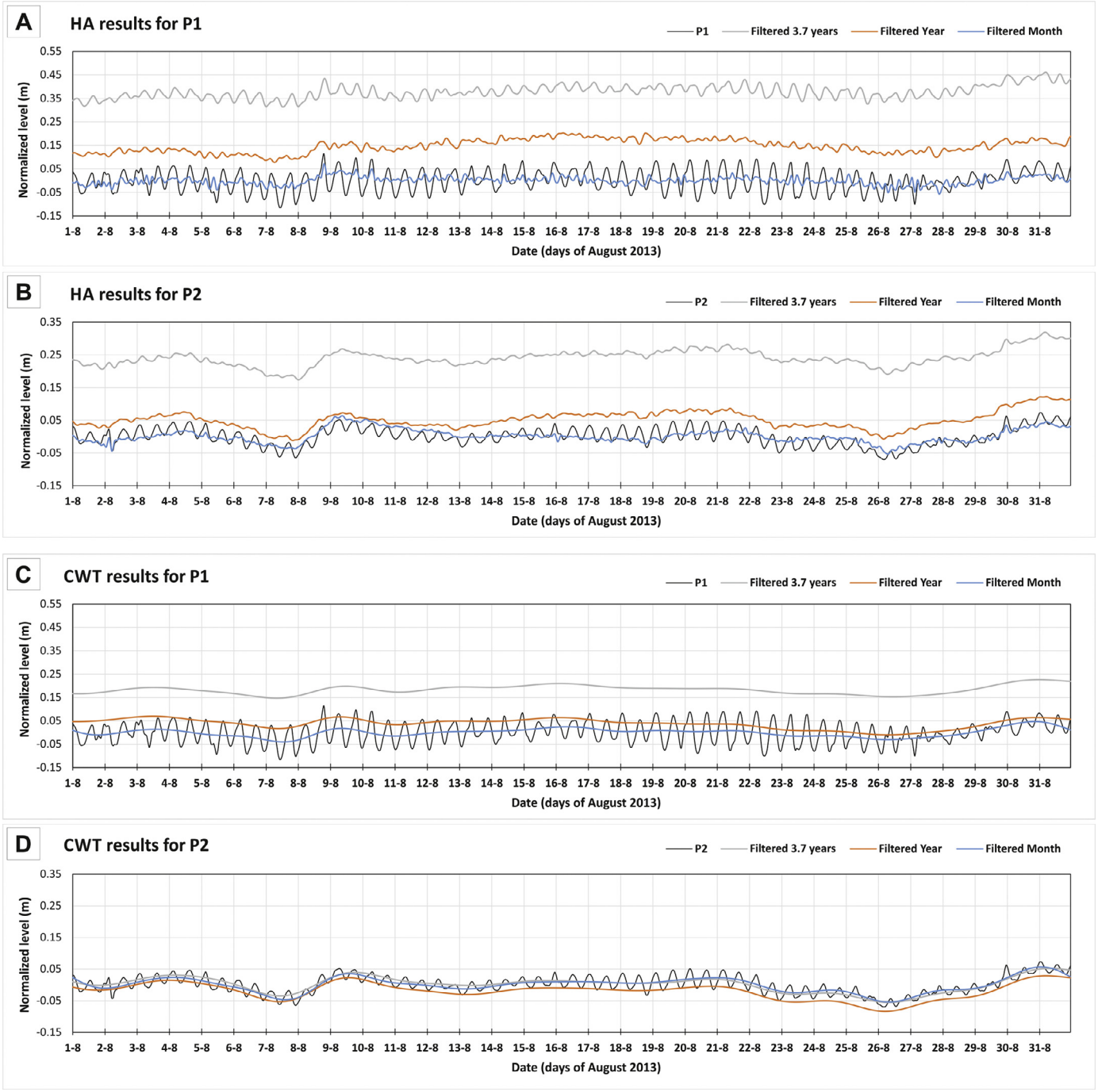

Fig. 8. 3.7 years and one month of filtered groundwater heads at P1 (A) and P2 (B) from the HA method (A-B) and the CWT method (C-D). The time series has been adjusted to one month to compare the filtered results of each time series length. The relative heads in one month and in the complete time series (left axis) do not overlap because the mean value in each time series length was removed prior to analysis. (For interpretation of the references to colour in this figure legend, the reader is referred to the web version of this article.)

6. Concluding remarks

Two methods, HA (Harmonic Analysis) and CWT (Continuous Wavelet Transform), were applied to filter groundwater heads affected by tidal oscillations with the aim of comparing the results and evaluating the best option for filtering. Both methods were applied to three time series of different lengths to assess their influences on the outcomes. The results showed that both tidal extraction methods yielded acceptable resolutions of the tidal part, allowing practically the entire extraction of the tidal constituents that could be found in the coastal groundwater head, although some discrepancies and failures were observed.

The filtering process using the HA method showed better results for the shorter time series (one month), even with the absence of the lowest tidal frequencies, which could not be fitted in that case. In the filtering processes for longer time series (one year and 3.7 years), the fits were incomplete because the semidiurnal tidal oscillations remained in the groundwater heads. The lowest tidal frequencies detected in those cases were fitted with the influence of the non-tidal oscillations because the amplitude values for the annual and semi-annual constituents (SA and SSA) were higher in both groundwater heads than in the tidal level. This produced an overestimation of the low-frequency tidal constituents, which could be addressed with a better knowledge of non-tidal processes

with longer periods that would allow the frequency resolution to be increased.

The results obtained by applying the CWT method showed better fits than the HA method at both high and low tidal frequencies in the groundwater heads for all the time series because both the tidal part and possible noise (oscillations below 1 h) were almost completely filtered. However, the CWT results showed a slight decoupling between the results of different time series due to the lack of adjustment at the lower frequencies (not detected in shorter records) but with a very slight coupling between the tidal and non-tidal low frequencies (i.e., low mixing between them).

The variations in groundwater head evolution at the two filtered points also means that the different depths of measurement strongly influenced the groundwater head measurements and therefore the filtering process. The proposed methods highlighted the effects caused by differences in depth from the shoreline, since the tidal constituents were better resolved at increasing depths in the aquifer. The methods also allowed the extraction of the tidal part of the signal even when that part was fairly low (P2). This means that the methods could be useful tools for filtering head datasets and could enable the better management of coastal aquifers through a complete analysis of time series.

Acknowledgements

The tidal dataset was supplied by State Harbours, Ministry of Public Services (government of Spain). This study was supported by project CGL2012-32892, which was funded by the Ministry of Science and Innovation (government of Spain) and research group RNM-369 of the regional government of Andalusia. We are very grateful to the editor and reviewers for their constructive comments, which considerably contributed to improving the quality of the final version of the manuscript. We would also like to thank Christine Laurin for editing the article.

Supplementary materials

Supplementary material associated with this article can be found, in the online version, at doi:10.1016/j.advwatres.2016.08.016.

References

Brown, J.M., Bolaños, R., Howarth, M.J., Souza, A.J., 2012. Extracting sea level residual in tidally dominated estuarine. Ocean Dyn. 62, 969–982. http://link.springer.com/article/10.1007%2Fs10236-012-0543-7.

Bye, J.A.T., Narayan, K.A., 2009. Groundwater response to the tide in wetlands: observations from the Gillman Marshes, South Australia. Estuarine, Coastal Shelf Sci. 84, 219–226. http://www.sciencedirect.com/science/article/pii/S0272771409002972.

Calvache, M.L., Ibáñez, P., Duque, C., López-Chicano, M., Martín-Rosales, W., González-Ramón, A., Rubio, J.C., Viseras, C., 2009. Numerical modelling of the potential effects of a dam on a coastal aquifer in S. Spain. Hydrol. Processes 23, 1268–1281 http://onlinelibrary.wiley.com/doi/10.1002/hyp.7234/abstract;jsessionid=99D77BF5F3863E553EC0B985E6C17A67.f04t04 .

Cartwright, N., Nielsen, P., Dunn, S., 2003. Water table waves in an unconfined aquifer: experiments, and modeling. Water Resour. Res. 39 (12), 1330. oi/10.1029/2003WR002185/abstract.

Chapuis, R.P., Bélanger, C., Chenaf, D., 2005. Pumping test in a confined aquifer under tidal influence. Ground Water 44 (2), 300–305. http://onlinelibrary.wiley.com/doi/10.1111/j.1745-6584.2005.00139.x/abstract.

Chattopadhyay, P.B., Vedanti, N., Singh, V.S., 2015. A conceptual numerical model to simulate aquifer parameters. Water Resour. Manage. 29, 771–784. http://link.springer.com/article/10.1007%2Fs11269-014-0841-6.

Chen, C., Jiao, J.J., 1999. Numerical simulation of pumping test in multilayer wells with non-Darcian flow in the wellbore. Ground Water 37 (3), 465–474. http://onlinelibrary.wiley.com/doi/10.1111/j.1745-6584.1999.tb01126.x/abstract.

Chen, Y.J., Chen, G.Y., Yeh, H.D., Jeng, D.S., 2011. Estimations of tidal characteristics and aquifer parameters via tide-induced head changes in coastal observation wells. Hydrol. Earth Syst. Sci. 15, 1473–1482. http://www.hydrol-earth-syst-sci.net/15/1473/2011/.

Codiga, D.L., 2011. Unified Tidal Analysis and Prediction Using the U_TIDE Matlab© Functions. Graduate School of Oceanography, University of Rhode Island, Narragansett, RI, p. 59. Technical Report 2011-01 http://www.po.gso.uri.edu/~codiga/utide/utide.htm .

Codiga, D.L., Rear, L.V., 2004. Observed tidal currents outside Block Island Sound: Offshore decay and effects of estuarine outflow. J. Geophys. Res. 109. http://onlinelibrary.wiley.com/doi/10.1029/2003JC001804/abstract.

Daubechies, I., Mallat, S., Willsky, A.S., 1992. Introduction to the special issue on wavelet transforms and multiresolution signal analysis. IEEE Trans. Inf. Theory 38 (2), 529–531. http://ssg.mit.edu/~willsky/publ_pdfs/99_pub_IEEE.pdf.

Doodson, A.T., 1954. Appendix to circular-letter 4-H. The harmonic development of the tide-generating potential. Int. Hydrographic Rev. 31, 37–61.

Duque, C., Calvache, M.L., Pedrera, A., Martín-Rosales, W., López-Chicano, M., 2008. Combined time domain electromagnetic soundings and gravimetry to determine marine intrusion in a detrital coastal aquifer (Southern Spain). J. Hydrol. 349, 536–547. http://www.sciencedirect.com/science/article/pii/S0022169407007081.

Duque, C., Calvache, M.L., Engesgaard, P., 2010. Investigating river–aquifer relations using water temperature in an anthropized environment (Motril-Salobreña aquifer). J. Hydrol. 381, 121–133. http://www.sciencedirect.com/science/article/pii/S0022169409007525.

Duque, C., López-Chicano, M., Calvache, M.L., Martin-Rosales, W., Gómez-Fontalva, J.M., Crespo, F., 2011. Recharge sources and hydrogeological effects of irrigation and an influent river identified by stable isotopes in the Motril-Salobreña aquifer (Southern Spain). Hydrol. Processes 25 (4), 2261–2274. http://onlinelibrary.wiley.com/doi/10.1002/hyp.7990/abstract.

Erol, S., 2011. Time-frequency analysis of tide-gauge sensor data. Sensors 11, 3939–3961. http://www.mdpi.com/1424-8220/11/4/3939.

Erskine, A., 1991. The effect of tidal fluctuation on a coastal aquifer in the UK. Ground Water 29 (4), 556–562. http://dx.doi.org/10.1111/j.1745-6584.1991.tb00547.x/abstract. http://onlinelibrary.wiley.com/doi/.

Farge, M., 1992. Wavelet transform and their applications to turbulence. Ann. Rev. Fluid Mech. 24, 395–457 http://www.annualreviews.org/doi/abs/10.1146/annurev.fl.24.010192.002143.

Ferris, J.G., 1952. Cyclic fluctuations of water level as a basis for determining aquifer transmissibility. IAHS Publ. 33, 148–155. https://pubs.er.usgs.gov/publication/70133368.

Flinchem, E.P., Jay, D.A., 2000. An introduction to wavelet transform tidal analysis methods. Estuarine Coastal Shelf Sci. 51 (2), 177–200. http://www.sciencedirect.com/science/article/pii/S0272771400905869.

Foreman, M.G.G., 1977. Manual for Tidal Heights Analysis and Prediction. Institute of Ocean Sciences, Patricia Bay, p. 101. Pacific Marine Science Report 77-10(Revised 2004) https://www.researchgate.net/publication/264782849_Manual_for_Tidal_Currents_Analysis_and_Prediction .

Foreman, M.G.G., Crawford, W.R., Marsden, R.F., 1995. De-Tiding: Theory and Practice, in: Quantitative Skill Assessment for Coastal Ocean Models, American Geophysical Union (AGU). John Wiley & Sons, Ltd, pp. 203–239. https://www.researchgate.net/publication/242203926_De-tiding'_Theory_and_Practice.

Godin, G., 1972. The Analysis of Tides. University of Toronto Press, Toronto, p. 264.

Guo, L., van der Wegen, M., Jay, D.A., Matte, P., Wang, Z.B., Roelvink, D., He, Q., 2015. River-tide dynamics: exploration of nonstationary and nonlinear tidal behavior in the Yangtze River estuary. J. Geophys. Res. Oceans 120. http://onlinelibrary.wiley.com/doi/10.1002/2014JC010491/abstract.

Jay, D.A., Flinchem, E.P., 1995. Wavelet transform analyses of non-stationary tidal currents. In: Proceedings of the Fifth Working Conference on Current Measurement. St. Petersburg, FL, IEEE, pp. 100–105. http://ieeexplore.ieee.org/xpl/articleDetails.jsp?arnumber=516158.

Jay, D.A., Flinchem, E.P., 1997. Interaction of fluctuating river flow with a barotropic tide: a demonstration of wavelet tidal analysis methods. J. Geophys. Res. 102 (C3), 5705–5720. http://onlinelibrary.wiley.com/doi/10.1029/96JC00496/abstract.

Jay, D.A., Flinchem, E.P., 1999. A comparison of methods for analysis of tidal records containing multi-scale non-tidal background energy. Cont. Shelf Res. 19 (13), 1695–1732. http://www.sciencedirect.com/science/article/pii/S0278434399000369.

Jha, M.K., Kamii, Y., Chikamori, K., 2003. On the estimation of phreatic aquifer parameters by the tidal response technique. Water Resour. Manage. 17, 69–88. http://link.springer.com/article/10.1023%2FA%3A1023018107685.

Kacimov, A., Abdalla, O., 2010. Water table response to a tidal agitation in a coastal aquifer: the Meyer-Polubarinova-Kochina theory revisited. J. Hydrol. 392, 96–104. http://www.sciencedirect.com/science/article/pii/S0022169410004798.

Landau, L.D., Lifshtiz, E.M., 1977. Quantum Mechanics. Pergamon Press, Oxford, pp. 46–48. https://archive.org/details/QuantumMechanics_104.

Leffler, K.E., Jay, D.A., 2009. Enhancing tidal harmonic analysis: Robust (hybrid L-1/L-2) solutions. Cont. Shelf Res. 29, 78–88. http://www.sciencedirect.com/science/article/pii/S0278434308001842.

Li, H., Jiao, J.J., 2003. Influence of the tide on the mean watertable in an unconfined, anisotropic, inhomogeneous coastal aquifer. Adv. Water Resour. 26, 9–16. http://www.sciencedirect.com/science/article/pii/S0309170802000970.

Licata, I.L., Langevin, C.D., Dausman, A.M., Alberti, L., 2011. Effect of tidal fluctuations on transient dispersion of simulated contaminant concentrations in coastal aquifers. Hydrogeol. J. 19, 1313–1322. http://link.springer.com/article/10.1007%2Fs10040-011-0763-9.

Matte, P., Jay, D.A., Zaron, E.D., 2013. Adaptation of Classical tidal harmonic analysis to nonstationary tides, with application to river tides. J. Atmos. Oceanic Technol. 30 (3), 569–589. http://journals.ametsoc.org/doi/abs/10.1175/JTECH-D-12-00016.1.

Millham, N.P., Howes, B.L., 1995. A comparison of methods to determine K in a shallow coastal aquifer. Ground Water 33 (1), 49–57. http://onlinelibrary.wiley.com/doi/10.1111/j.1745-6584.1995.tb00262.x/abstract.

Nielsen, P., 1990. Tidal dynamics of the water table in beaches. Water Resour. Res. 26 (9), 2127–2134. http://onlinelibrary.wiley.com/doi/10.1029/WR026i009p02127/abstract.

Nielsen, P., Aseervatham, R., Fenton, J.D., Perrochet, P., 1997. Groundwater waves in aquifers of intermediate depths. Adv. Water Resour. 20 (1), 37–43. http://www.sciencedirect.com/science/article/pii/S0309170896000152.

Parker, B.B., 2007. Tidal Analysis and Prediction. NOAA Special Publication NOS CO-OPS 3 http://tidesandcurrents.noaa.gov/publications/Tidal_Analysis_and_Predictions.pdf .

Pawlowicz, R., Beardsley, B., Lentz, S., 2002. Classical tidal harmonic analysis including error estimates in Matlab© using T_TIDE. Comput. Geosci. 28, 929–937. http://www.sciencedirect.com/science/article/pii/S0098300402000134.

Singh, A., Jha, M.K., 2013. Efficacy of tide-aquifer interaction models for characterizing coastal aquifer systems. In: Ramkumar, Mu. (Ed.), On a Sustainable Future of the Earth's Natural Resources. Springer Earth System Sciences http://link.springer.com/chapter/10.1007%2F978-3-642-32917-3_25.

Teo, H.T., Jeng, D.S., Seymour, B.R., Barry, D.A., Li, L., 2003. A new analytical solution for water table fluctuations in coastal aquifers with sloping beaches. Adv. Water Resour. 26 (12), 1239–1247. http://www.sciencedirect.com/science/article/pii/S0309170803001313.

Torrence, C, Compo, G, 1998. A practical guide to wavelet analysis. Bull. Am. Meteorol. Soc. 79 (1), 61–78. http://journals.ametsoc.org/doi/abs/10.1175/1520-0477(1998)079%3C0061%3AAPGTWA%3E2.0.CO%3B2.

Trefry, M.G., Bekele, E., 2004. Structural characterization of an island aquifer via tidal methods. Water Resour. Res. 40 (1). http://onlinelibrary.wiley.com/doi/10.1029/2003WR002003/abstract.

Trefry, M.G., Johnston, C.D., 1998. Pumping test analysis for a tidally forced aquifer. Ground Water 36 (3), 427–433. http://onlinelibrary.wiley.com/doi/10.1111/j.1745-6584.1998.tb02813.x/abstract.

Vianna, M.L., Menezes, V.V., 2005. Singular spectrum analysis of nonstationary tidal currents applied to ADCP data from the Northeast Brazilian Shelf. J. Atmos. Oceanic Technol. 23, 138–151. http://journals.ametsoc.org/doi/abs/10.1175/JTECH1824.1.

Wu, L., 2009. Experimental research on effect of tide for alongshore groundwater table. In: Advances in Water Resources and Hydraulic Engineering, Proceedings of 16th IAHR-APD Congress and 3rd Symposium of IAHR-ISHS, 2009. Springer Berlin, Heidelberg, pp. 785–788. http://link.springer.com/chapter/10.1007%2F978-3-540-89465-0_138.

Zhou, X., 2008. Determination of aquifer parameters based on measurements of tidal effects on a coastal aquifer near Beihai, China. Hydrol. Processes 22, 3176–3180. http://onlinelibrary.wiley.com/doi/10.1002/hyp.6906/abstract.